 doi:10.20944/preprints202012.0169.v1

Article

Physiological and comparative proteomic analyses provide insight into the differential responses of *Acanthus ilicifolius* and its relative, *Acanthus mollis*, to tidal flooding stress

Yi-ling Liu[1], Hai-lei Zheng[1]*

[1] Key Laboratory of the Ministry of Education for Coastal and Wetland Ecosystems, College of the Environment and Ecology, Xiamen University, Xiamen, Fujian 361005, P.R. China

* Correspondence: zhenghl@xmu.edu.cn; Tel.

Abstract: The mangrove plant *Acanthus ilicifolius* and its relative, *A. mollis*, have been previously proved to possess diverse pharmacological effects. Therefore, evaluating the differentially expressed proteins of these species under tidal flooding stress is essential to fully exploit and benefit from their medicinal values. The roots of *A. ilicifolius* and *A. mollis* were exposed to 6 h of flooding stress per day for 10 days. The dry weight, hydrogen peroxide (H_2O_2) content, anatomical characteristics, carbon and energy levels, and two-dimensional electrophoresis coupled with MALDI-TOF/TOF MS technology were used to reveal the divergent flooding resistant strategies. *A. ilicifolius* performed better under tidal flooding stress, which was reflected in the integrity of the morphological structure, more efficient use of carbon and energy, and a higher percentage of up-regulated proteins associated with carbon and energy metabolism. *A. mollis* could not survive in flooding conditions for a long time, as revealed by incomplete cell structures of the roots, less efficient use of carbon and energy, and a higher percentage of down-regulated proteins associated with carbon and energy metabolism. Energy provision and flux balance played a role in the flooding tolerance of *A. ilicifolius* and *A. mollis*.

Keywords: Acanthus species; flooding stress; physiological; comparative proteomics analyses; carbon and energy metabolism

1. Introduction

The physical characteristics of soil influence a variety of physiological and biochemical processes of plants. The leaves and roots of terrestrial plants absorb molecular oxygen from air and land, respectively [1]. Previous studies have shown that flooding stress is a widespread phenomenon that inhibits plant growth and production [2]. Continuous and heavy rainfall causes soil pores saturated with excess water, inducing oxygen deficiency in plant roots [1-2]. Meanwhile, the roots that are subjected to flooding stress may inhibit photosynthesis, including a decrease of photosynthetic electron transport chain and an increase in the level of reactive oxygen species (ROS) [3]. A shift of aerobic respiration to anaerobic respiration reduced the availability of the adenosine triphosphate (ATP) in plants [4] and increasing the content of ethanol [5].

Some plants have evolved morphological, physiological, and metabolic adaptation strategies to ensure survival under flooding stress [6-7]. For example, maize develops an extensive aerenchyma system to facilitate gas transport apart from adventitious roots [6]. Rice retains a gas-associated film to facilitate oxygen uptake to survive under flooding [7]. Mangrove plants, such as *Kandelia obovata*, *Sonneratia apetala*, *Aeguceras corniculatum*, and *Rhizophora stylosa* develop specialized roots for gaseous exchange [8]. Soybean (PELBR10-6000) increased the level of CO_2 assimilation rate and readily responded to the lack of energy by activating the fermentative enzymes and alanine aminotransferase during the recovering period [9], indicating that the capacity to quickly resume the normal energy level is crucial in tolerating flooding stress [10].

Preprints (www.preprints.org) | NOT PEER-REVIEWED | Posted: 7 December 2020 doi:10.20944/preprints202012.0169.v1

A comparative study of species is one of the important methods to determine the mechanism of stress-resistant. The difference in fermentative enzymes and alanine aminotransferase activity resulted in different responses to energy deficiency between two soybean genotypes under flooding conditions [9]. A comparison of *Alternanthera philoxeroides* with *Hemarthria altissim*a showed that plants could adapt to wetland habitats, in which water levels fluctuate, by maintaining the functionality of the photosynthetic apparatus [11]. Waterlogged *Phalaris aquatica* and *Festuca arundinacea* regained growth during the recovery period compared with *Dactylis glomerata* and *Bromus catharticus* [12]. In addition, the favorable alleles of related species are more comfortable to introduce to improve crops [13]. The transfer of resistance genes between *Sinapis alba* and *Brassica* species by somatic and sexual hybridization has been accomplished [14].

The mangrove plant, *Acanthus ilicifolius*, has remarkable morphology and physiology [15]. *A. ilicifolius* is mainly distributed in Australia, Australasia, and the southeastern Asia intertidal zone and has numerous medicinal properties [16]. Previous findings showed that untreated or submerged *A. ilicifolius* over 3 h per day was not conducive to the growth [17]. Meanwhile, the effect of flooding stress on *A. ilicifolius* at the molecular level is not well elucidated. *Acanthus* belongs to the Acanthaceae family and is the only genus that comprises of both terrestrial and aquatic species [15]. As the *Acanthus* model plant, *A. mollis* is native to the Mediterranean region from central Europe and northwest Africa [18]. *A. mollis* was recently introduced into China and used as a medicinal plant in traditional medicine [18-19]. The extracts of *A. mollis* tissues have been used for the treatment of inflammation and cancer problems [20]. However, the flooding tolerance of *A. mollis* has not yet been described. Since non-model plants lack a genetic transformation system to elucidate the metabolic mechanism, proteome and transcriptome are useful to provide powerful information about the metabolic pathways of non-model plants. The protein, as the functional executor, is closely related to physiological changes. In our previous study, we have reported the flooding tolerance of the leaves of *Avicennia marina* using comparative proteomic analyses [21]. Hence, evaluating the differentially expressed proteins (DEPs) of *A. ilicifolius* and *A. mollis* under tidal flooding stress is essential to fully exploit and benefit from their medicinal values.

Paraffin sections, physiological index measurements, and two-dimensional electrophoresis (2-DE) technique were performed on the leaves and roots of *A. ilicifolius* and *A. mollis* under tidal flooding stress. Our results first provide the anatomical characteristics, carbon and energy levels, and proteomic information about *A. ilicifolius* and its relative, *A. mollis*, under tidal flooding stress.

2. Results

2.1. Relative dry weight and H_2O_2 content of Acanthus species under tidal flooding stress

The two species changed the relative dry weight and H_2O_2 content to differing extents under tidal flooding stress. The relative dry weight of *A. ilicifolius* was increased in both the leaf and root tissues (Fig. 1A) but with no significant differences. The relative H_2O_2 content was significantly decreased on the tenth day in *A. ilicifolius* leaves and showed no significant differences from day 4-12 in *A. ilicifolius* roots (Fig. 1C). Tidal flooding treatment significantly decreased the relative dry weight (Fig. 1B) and increased the relative H_2O_2 content of *A. mollis* in both tissues (Fig. 1D). Overall, the relative dry weight (expressed as a percentage of the control) of *A. ilicifolius* was significantly higher compared to that of *A. mollis* from day 8-12.

Preprints (www.preprints.org) | NOT PEER-REVIEWED | Posted: 7 December 2020 doi:10.20944/preprints202012.0169.v1

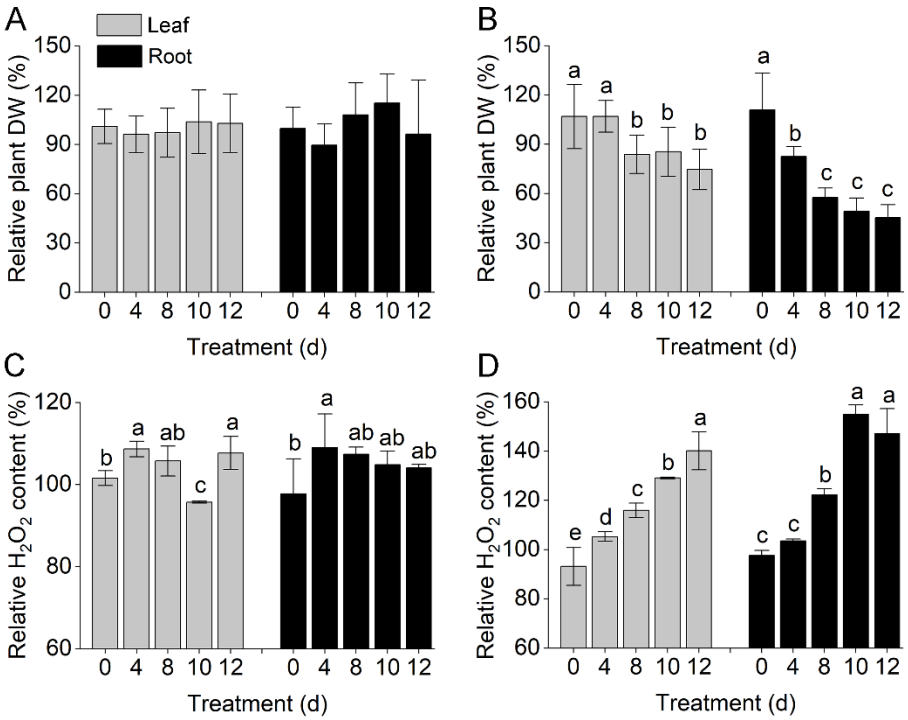

Figure 1. (A) Relative plant dry weight of *A. ilicifolius*. (B) Relative plant dry weight of *A. mollis*. (C) Relative H_2O_2 content of *A. ilicifolius*. (D) Relative H_2O_2 content of *A. mollis*. Grey represents leaves; black represents roots. No significant differences were noted among the groups in (A). Data are shown as means ± SD from three independent biological replicates. The different letters indicate significant changes according to one-way ANOVA followed by Tukey's multiple range test ($P < 0.05$).

2.2. Effect of tidal flooding on the phenotype and anatomical characteristics of Acanthus species

The phenotype and anatomical characteristics of the two species are shown in Fig. 2. After 10 days of tidal flooding treatment, there was no significant change in *A. ilicifolius* (Fig. 2A1, B1), while the length of *A. mollis* roots became *shorter* (Fig. 2C1, D1).

The leaf blade of *A. ilicifolius* consisted of the upper epidermis, upper multiple epidermises, palisade parenchyma, spongy parenchyma, lower epidermis, and salt gland (Fig. 2A2), whereas that of *A. mollis* showed a different structure. The upper and lower epidermises of *A. mollis* were all single-layered and had glandular trichome (Fig. 2C2). *A. ilicifolius* roots consisted of the endodermis, epidermis, xylem, phloem, pith, cortex, lenticel, and periderm (Fig. 2A4, A5) whereas the roots of *A. mollis* contained periderm cells (Fig 2 D5).

In the leaf blade of *A. ilicifolius*, the vein phloem possessed a hollow cavity that was enlarged after tidal flooding treatment (Fig. 2B3). The control group of *A. mollis* exhibited schizogenous aerenchyma in the leaf vein, which disappeared after tidal flooding treatment. The periderm is a secondary protective tissue that protects plant roots from bacterial infections [22]. In *A. mollis* roots, the pith parenchyma cells were damaged and the periderm cells were ruptured under tidal flooding stress (Fig. 2D4, D5).

Preprints (www.preprints.org) | NOT PEER-REVIEWED | Posted: 7 December 2020 doi:10.20944/preprints202012.0169.v1

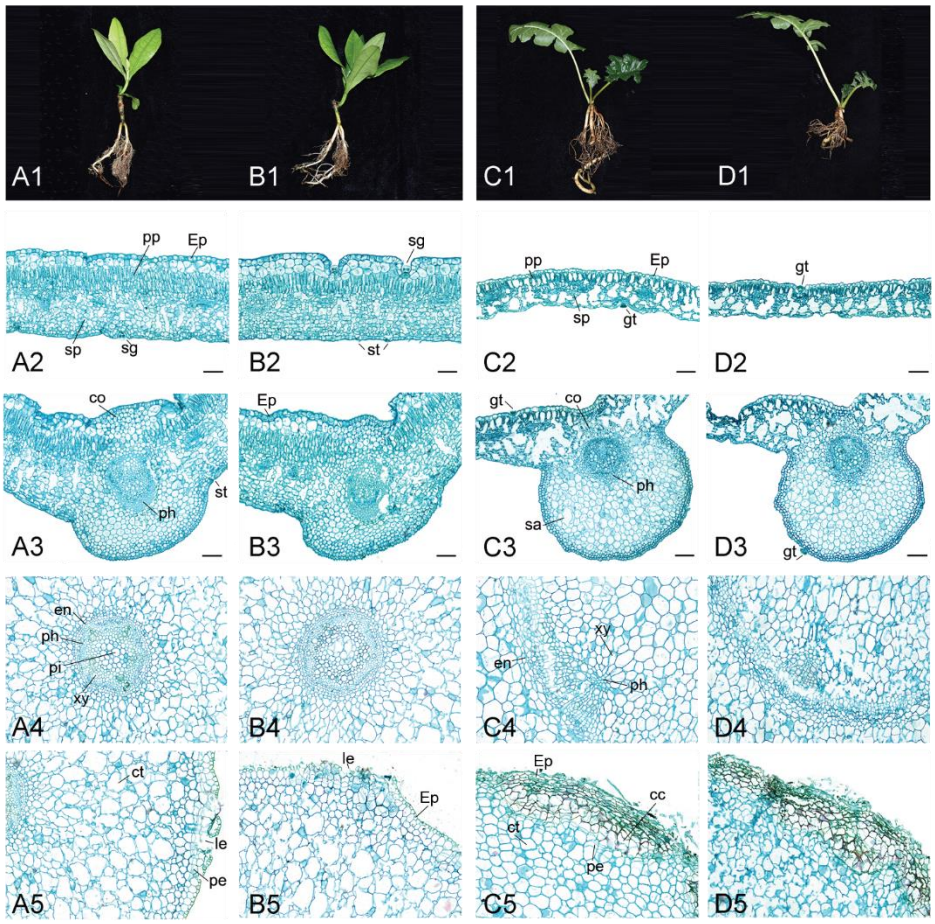

Figure 2. Phenotypic and anatomical changes of *A. ilicifolius* and *A. mollis* exposed to tidal flooding stress. (A1-A5) *A. ilicifolius* plants on control treatment, (B1-B5) *A. ilicifolius* plants under tidal flooding stress, (C1-C5) *A. mollis* plants on control treatment, (D1-D5) *A. mollis* plants under tidal flooding stress. Row 1: the phenotypic of Acanthus species, Row 2: the cross-section of the leaf blade, Row 3: the main vein of the leaf, Row 4: stele of root, Row 5: epidermis of root. Root sections, about 5 cm from root tip, photos of optical microscopes. Cross-sections with thickness of 10 mm were made and stained with safranine and fast green. cc: cork cambium; co: collenchyma; ct: cortex; en: endodermis; Ep: epidermis; gt: glandular trichome; le: lenticel; pe: periderm; ph: phloem; pi: pith; pp: palisade parenchyma; sa: schizogenous aerenchyma; st: stomata; sp: lacunar parenchyma; xy: xylem. Bars: 100 μm.

2.3. Identification and quantification of tidal flooding-responsive proteins

Representative 2-DE gels of the leaves and roots of the two species are shown in Supplemental Fig. S3. In *A. ilicifolius*, approximately 78 and 40 spots were identified from leaves and roots, respectively (Fig. 3A, B; Table 1, 2; Supplementary Table S2). In *A. mollis*, about 67 and 45 spots were identified from leaves and roots, respectively (Fig. 3C, D; Table 3, 4; Supplementary Table S2).

To understand the global relationship between samples, PCA was performed to evaluate the similarity between the samples (Fig. 4). The weights of the first principal component (PC1) satisfied the cumulative percent variance (70-85%) [23], accounting for nearly 80% of the difference. The control group (CK) and the soil flooding group (SF) separated from each other. The excellent biological repeatability of these proteomes, derived from the same condition, indicates a stable and distinct response of *A. ilicifolius* and *A. mollis* to tidal flooding treatment.

Preprints (www.preprints.org) | NOT PEER-REVIEWED | Posted: 7 December 2020 doi:10.20944/preprints202012.0169.v1

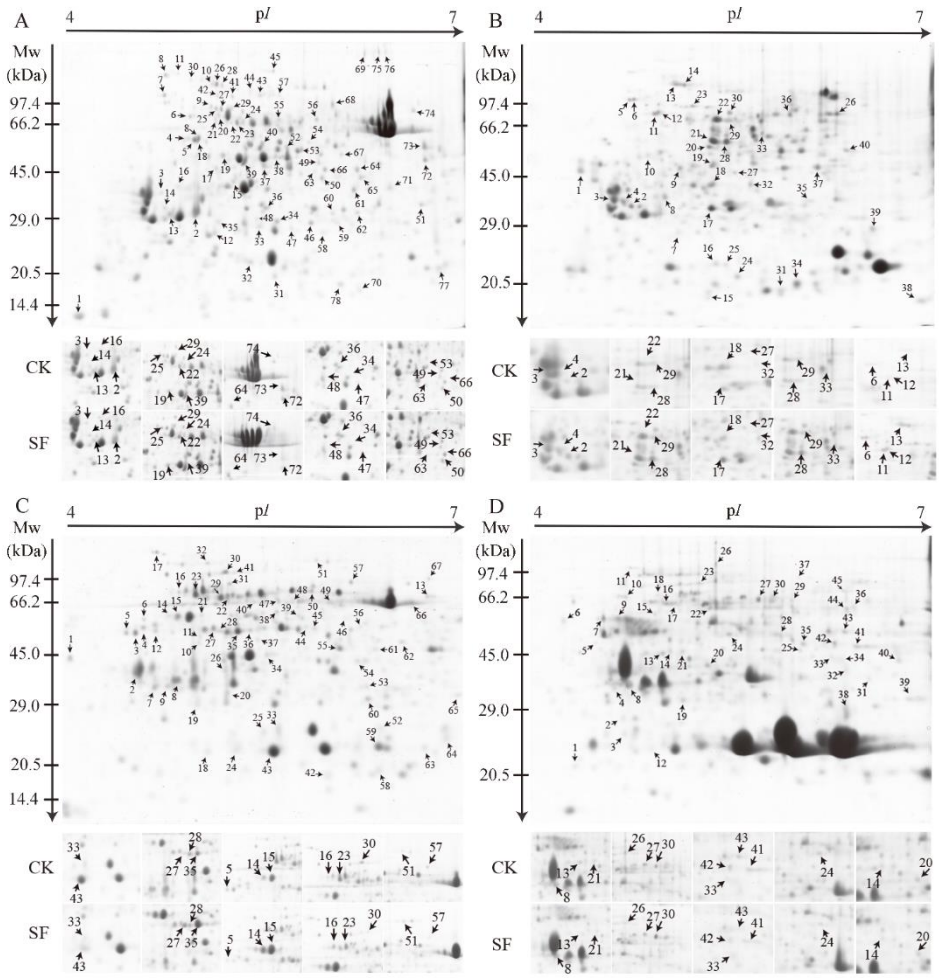

Figure 3. Two-dimensional (2-DE) analysis of proteins extracted from (A) *A. ilicifolius* leaves, (B) *A. ilicifolius* roots, (C) *A. mollis* leaves, (D) *A. ilicifolius* roots. The numbers correspond with the spot ID, mentioned in Table 1-4. The isoelectric point (p*I*) and molecular weight (MW) in kilodaltons are indicated on the top and left of the gel, respectively. CK and SF represent the control group and soil tidal flooding stress, respectively.

2.4. Functional classification of DEPs

More proteins were up-regulated in *A. ilicifolius* than in *A. mollis* tissues (Fig. 5). A higher percentage of up-regulated proteins were found in carbon and energy metabolism and amino acid and protein metabolism in *A. mollis* leaves, while in transcription and signal transduction in *A. ilicifolius* leaves. In addition, *A. ilicifolius* leaves had a lower percentage of up-regulated proteins associated with stress and defense. Overall, *A. ilicifolius* tissues had a high percentage of up-regulated proteins and a low percentage of down-regulated proteins associated with carbon and energy metabolism. Meanwhile, a higher percentage of down-regulated proteins of *A. mollis* leaves were associated with carbon and energy metabolism, stress and defense, and transcription and signal transduction (Fig. 5).

Compared with *A. mollis* roots, a higher percentage of up-regulated proteins of *A. ilicifolius* roots were associated with carbon and energy metabolism, amino acid and protein metabolism, stress and defense, and transcription and signal transduction. In *A. mollis* roots, there was a higher percentage of down-regulated proteins in all pathways (Fig. 5).

Preprints (www.preprints.org) | NOT PEER-REVIEWED | Posted: 7 December 2020 doi:10.20944/preprints202012.0169.v1

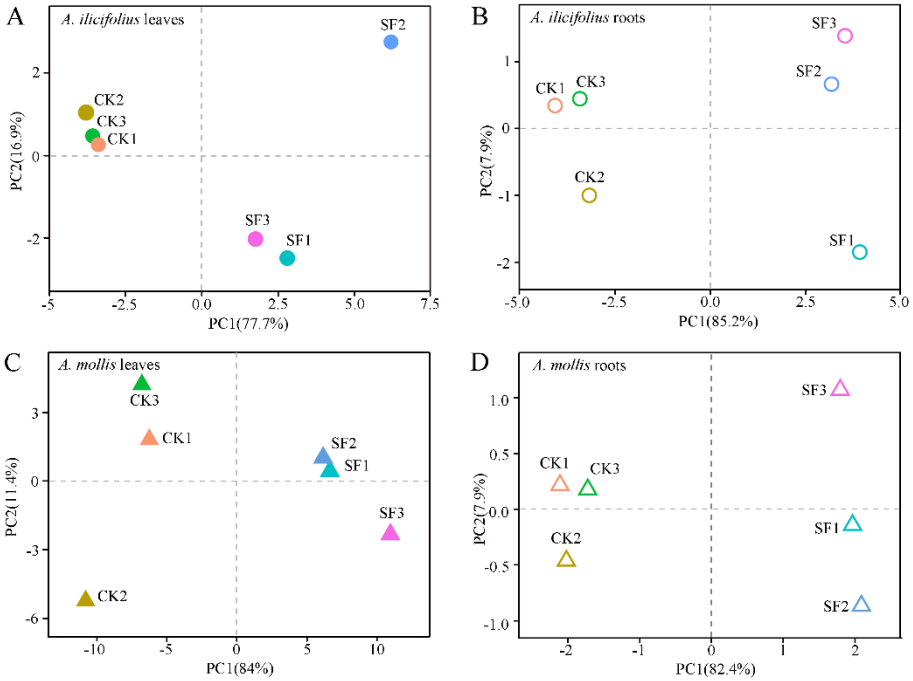

Figure 4. Principal Component Analysis (PCA) of total proteome data for (A) *A. ilicifolius* leaves, (B) *A. ilicifolius* roots, (C) *A. mollis* leaves, (D) *A. mollis* roots. Percentage variance for each principal component is given.

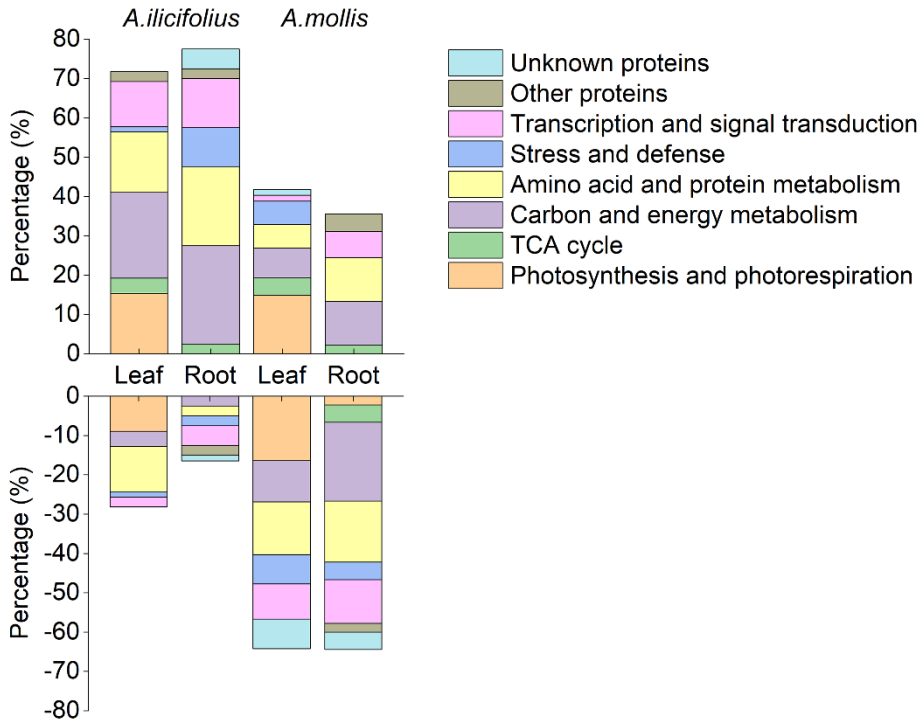

Figure 5. Functional classification analysis of DEPs of *A. ilicifolius* and *A. mollis*. The detailed information for each spots is shown in Table 1-4.

 doi:10.20944/preprints202012.0169.v1

1

Table 1. Identification of DEPs of *A. ilicifolius* leaves with an expression change greater than 2.0-fold change under tidal flooding stress

Spot [a]	Accession (gb) [b]	Protein Name [c]	Thero. [d] kDa/p*I*	Exper. [e] kDa/p*I*	Score [f]	MP [g]	Species [h]	SF vs. CK [i]
Photosynthesis and photorespiration								
1	gi|222842405	Plastocyanin family protein	17.07/4.94	6.80/4.00	98	2	*Populus trichocarpa*	-6.268
2	gi|449515811	Predicted: chlorophyll a-b binding protein 40, chloroplastic-like, partial	15.98/6.58	18.87/4.93	88	2	*Cucumis sativus*	-1.555
12	gi|222859802	Chlorophyll a-b binding protein 2	28.09/5.29	15.44/5.07	87	6	*Populus trichocarpa*	1.937
13	gi|475542040	Chlorophyll a-b binding protein, chloroplastic	28.72/5.14	19.47/4.74	114	6	*Aegilops tauschii*	3.202
16	gi|449442663	Predicted: phosphoglycolate phosphatase-like	41.72/6.47	24.00/4.78	63	3	*Cucumis sativus*	3.455
18	gi|474352688	Oxygen-evolving enhancer protein 1, chloroplastic	34.64/5.75	36.97/4.93	352	7	*Triticum urartu*	2.893
33	gi|223540996	Chlorophyll a/b binding protein, putative	31.10/5.52	16.37/5.43	75	5	*Ricinus communis*	-1.887
58	gi|428230860	Chlorophyll binding protein, partial	21.39/5.19	15.41/5.93	66	2	*Clermontia arborescens* subsp. *Waihiae*	6.846
65	gi|475616276	Putative quinone-oxidoreductase-like protein, chloroplastic	35.43/9.13	27.96/5.86	69	11	*Aegilops tauschii*	-2.415
71	gi|550338673	Chain A family protein	40.79/8.54	23.76/6.45	70	10	*Populus trichocarpa*	-6.268
Calvin cycle								
4	gi|475522663	Ribulose bisphosphate carboxylase/oxygenase activase B, chloroplastic	51.47/8.86	38.41/4.86	268	5	*Aegilops tauschii*	-5.046

 doi:10.20944/preprints202012.0169.v1

5	gi|508726181	Rubisco activase isoform 2	52.37/5.26	37.73/4.91	407	10	*Theobroma cacao*	1.103
7	gi|508787184	RuBisCO large subunit-binding protein subunit alpha isoform 1	64.07/5.06	58.37/4.67	108	9	*Theobroma cacao*	1.518
9	gi|502125499	Predicted: ruBisCO large subunit-binding protein subunit beta, chloroplastic-like	63.20/5.85	52.72/5.05	162	6	*Cicer arietinum*	5.431
15	gi|542718032	Ribulose-1,5-bisphosphate carboxylase/oxygenase large subunit, partial (chloroplast)	38.09/6.49	25.25/5.22	294	11	*Prunus wilsoni*	3.362
19	gi|410927414	Chloroplast ribulose bisphosphate carboxylase/oxygenase activase beta1, partial	33.16/5.09	32.55/5.14	274	4	*Gossypium barbadense*	1.568
39	gi|223541989	Phosphoribulose kinase, putative	45.22/5.83	30.46/5.31	302	11	*Ricinus communis*	2.349
51	gi|399139809	Ribulose-1,5-bisphosphate carboxylase/oxygenase large subunit, partial	51.58/6.30	20.22/6.70	388	9	*Strobilanthes glutinosus*	-3.465
61	gi|406366546	Ribulose-1,5-bisphosphate carboxylase/oxygenase small subunit, partial (chloroplast)	19.30/8.80	23.30/6.17	61	8	*Gossypium gossypioides*	1.000
Carbon metabolism								
34	gi|449458564	Predicted: triosephosphate isomerase, chloroplastic-like	33.00/7.01	17.22/5.56	81	4	*Cucumis sativus*	1.349
38	gi|317373797	Chloroplast phosphoglycerate kinase 3	50.28/6.69	32.06/5.55	121	10	*Helianthus annuus*	1.671
46	gi|527186354	Triosephosphate isomerase	33.67/6.90	16.94/5.83	314	6	*Genlisea aurea*	3.564
48	gi|332005925	6-phosphogluconolactonase 4	29.51/6.23	17.67/5.40	91	2	*Arabidopsis thaliana*	2.677
49	gi|222864107	Cytosolic phosphoglycerate kinase family protein	42.77/5.70	30.36/5.89	314	7	*Populus trichocarpa*	2.056

 doi:10.20944/preprints202012.0169.v1

52	gi|223547261	Phosphoglycerate kinase, putative	50.11/8.74	35.17/5.64	95	2	*Ricinus communis*	1.764
56	gi|350538295	Enolase	48.05/5.68	46.18/5.87	233	8	*Solanum lycopersicum*	2.329
68	gi|485820030	Enolase, partial	11.86/7.98	41.86/5.95	84	3	*Schiedea heller*	2.103
73	gi|508711124	Glyceraldehyde-3-phosphate dehydrogenase A subunit2	43.26/8.15	35.69/6.73	407	11	*Theobroma cacao*	-2.508
75	gi|413916139	Glycine cleavage complex P-protein	119.11/6.79	88.83/6.36	118	8	*Zea mays*	2.887
76	gi|413916139	Glycine cleavage complex P-protein	119.11/6.79	89.61/6.42	99	8	*Zea mays*	3.691
TCA cycle								
63	gi|332189573	Malate dehydrogenase	35.89/6.11	28.43/5.94	70	7	*Arabidopsis thaliana*	1.083
64	gi|223526678	Malate dehydrogenase, putative	35.98/6.40	28.39/6.19	183	2	*Ricinus communis*	1.026
74	gi|499138229	Dihydrolipoamide dehydrogenase, partial	43.94/7.79	50.17/6.64	145	4	*Rhizophora stylosa*	1.362
		Energy metabolism						
6	gi|449454235	Predicted: V-type proton ATPase subunit B 1-like	54.36/4.96	47.50/4.88	103	10	*Cucumis sativus*	1.704
21	gi|545719412	ATP synthase CF1 alpha subunit (chloroplast)	55.57/5.15	48.13/5.10	547	18	*Allosyncarpia ternata*	3.568
23	gi|393396089	ATP synthase CF1 beta subunit (chloroplast)	53.80/5.20	44.61/5.25	774	18	*Vigna unguiculata*	1.176
24	gi|449434570	Predicted: ATP synthase subunit beta, mitochondrial-like	59.89/5.90	45.30/5.29	571	16	*Cucumis sativus*	-1.176
32	gi|508726652	ATP synthase D chain, mitochondrial	19.65/0.00	11.60/5.35	98	5	*Theobroma cacao*	-4.169
43	gi|350537279	Vacuolar H^+-ATPase A2 subunit isoform	68.96/5.30	58.53/5.43	534	19	*Solanum lycopersicum*	1.026
44	gi|350537129	Vacuolar H^+-ATPase A1 subunit	68.81/5.20	60.95/5.35	268	14	*Solanum*	3.239

 doi:10.20944/preprints202012.0169.v1

		isoform					*lycopersicum*	
45	gi|223550217	ATP-dependent clp protease, putative	103.12/6.27	73.67/5.53	382	19	*Ricinus communis*	1.578
50	gi|222848536	ATP synthase gamma chain 1 family protein	41.36/8.16	26.16/5.92	263	6	*Populus trichocarpa*	1.438
Amino acid and protein metabolism								
8	gi|449442347	Predicted: stromal 70 kDa heat shock-related protein, chloroplastic-like	75.46/5.18	70.85/4.68	67	7	*Cucumis sativus*	2.747
10	gi|332003097	Heat shock cognate protein 70-1	71.71/5.03	64.76/5.05	322	16	*Arabidopsis thaliana*	4.142
11	gi|460369188	Predicted: stromal 70 kDa heat shock-related protein, chloroplastic-like	74.96/5.20	72.88/4.79	97	3	*Solanum lycopersicum*	2.282
17	gi|508722909	20S proteasome alpha subunit F2	33.23/4.76	28.45/5.08	120	4	*Theobroma cacao*	2.319
25	gi|508784980	TCP-1/cpn60 chaperonin family protein	64.51/5.62	50.84/5.08	374	6	*Theobroma cacao*	-2.677
26	gi|508726275	Heat shock cognate protein 70-1	71.75/5.03	64.94/5.09	646	19	*Theobroma cacao*	1.306
27	gi|508784980	TCP-1/cpn60 chaperonin family protein	64.51/5.62	50.98/5.12	503	15	*Theobroma cacao*	-2.093
28	gi|293334615	Heat shock cognate 70 kDa protein 2	71.52/5.13	64.16/5.13	329	13	*Zea mays*	1.565
29	gi|332643321	Heat shock protein 60	61.58/5.66	52.08/5.21	163	7	*Arabidopsis thaliana*	6.843
35	gi|223544718	Groes chaperonin, putative	26.58/8.89	17.09/5.10	61	5	*Ricinus communis*	-3.754
37	gi|425856442	Mta/sah nucleosidase, partial	23.86/5.67	29.25/5.46	69	2	*Galium verum var. asiaticum*	1.668
53	gi|343465772	Plastid glutamine synthetase isoform	47.02/5.75	34.37/5.76	182	7	*Secale cereale x*	2.960

 doi:10.20944/preprints202012.0169.v1

							Triticum durum	
54	gi|332642427	S-adenosyethionine synthase 4	43.17/5.51	37.04/5.81	193	8	*Arabidopsis thaliana*	-1.269
55	gi|475453557	26S protease regulatory subunit 6B-like protein	30.13/6.54	46.00/5.57	155	9	*Aegilops tauschii*	-1.781
57	gi|475603792	Heat shock 70 kDa protein, mitochondrial	72.91/5.53	58.32/5.58	113	5	*Aegilops tauschii*	-2.900
59	gi|332646593	Proteasome subunit beta type-1	24.86/6.95	16.99/6.04	149	4	*Arabidopsis thaliana*	2.448
66	gi|550319185	Glutamate-ammonia ligase family protein	39.42/5.95	32.83/6.07	153	7	*Populus trichocarpa*	1.970
67	gi|332642304	Mitochondrial processing peptidase alpha subunit	54.19/6.04	39.89/6.12	104	2	*Arabidopsis thaliana*	1.262
69	gi|449450860	Elongation factor 2-like	95.03/5.97	86.42/6.25	133	8	*Cucumis sativus*	-3.222
77	gi|226491656	Peptidyl-prolyl cis-trans isomerase	26.37/0.00	10.97/6.84	155	6	*Zea mays*	-1.714
78	gi|543177006	Peptidyl-prolyl cis-trans isomerase	27.37/9.46	17.33/6.99	277	4	*Phaseolus vulgaris*	-5.867
Stress and defense								
36	gi|474311703	L-ascorbate peroxidase 1, cytosolic	27.56/5.85	18.92/5.45	117	5	*Triticum urartu*	1.505
70	gi|436805717	Copper/zinc-superoxide dismutase	15.39/5.47	8.88/6.22	96	2	*Litchi chinensis*	-6.172
Transcription and signal transduction								
3	gi|26454609	14-3-3 protein 7	28.91/4.96	22.71/4.65	137	3	*Solanum lycopersicum*	2.365
14	gi|449469841	Predicted: 14-3-3-like protein-like	29.64/4.77	19.79/4.67	90	3	*Cucumis sativus*	1.661
22	gi|508718683	Tubulin alpha-5	54.00/4.98	44.65/5.20	433	10	*Theobroma cacao*	1.983
30	gi|449464210	Predicted: leukotriene A-4 hydrolase homolog	69.93/5.37	67.72/4.88	157	5	*Cucumis sativus*	1.890

 doi:10.20944/preprints202012.0169.v1

31	gi|508782306	Eukaryotic translation initiation factor 5A-1	17.77/5.60	10.09/5.55	115	3	*Theobroma cacao*	1.953
40	gi|386278562	Actin7a, partial	39.39/5.21	36.73/5.45	271	9	*Vernicia fordii*	1.136
41	gi|223540420	Cell division protein ftsH, putative	75.50/6.43	57.28/5.21	467	7	*Ricinus communis*	2.854
42	gi|475605012	Cell division protease ftsH-like protein, chloroplastic	71.94/5.60	57.89/5.09	271	8	*Aegilops tauschii*	2.976
47	gi|15237579	RNA-binding protein NOB1	67.08/5.55	16.04/5.67	61	14	*Arabidopsis thaliana*	2.558
62	gi|355477483	F-box family protein	19.67/4.56	18.75/6.20	63	2	*Medicago truncatula*	-1.196
72	gi|514725733	Predicted: chloroplast stem-loop binding protein of 41 kDa, chloroplastic-like	41.49/6.41	31.25/6.73	203	6	*Setaria italica*	-1.133
Others proteins								
20	gi|508727025	Phosphate transporter traffic facilitator isoform 2	34.31/6.46	46.38/5.08	62	6	*Theobroma cacao*	4.787
60	gi|502120213	Predicted: flocculation protein FLO11-like isoform X2	66.28/10.59	18.40/5.99	69	4	*Cicer arietinum*	5.023

 doi:10.20944/preprints202012.0169.v1

Table 2. Identification of DEPs of *A. ilicifolius* roots with an expression change greater than 2.0-fold change under tidal flooding stress

Spot [a]	Accession (gb)[b]	Protein Name [c]	Thero. [d] kDa/p*I*	Exper. [e] kDa/p*I*	Score [f]	MP [g]	Species [h]	SF vs. CK [i]
TCA cycle								
R37	gi|226503019	Malate dehydrogenase, cytoplasmic	35.84/5.76	13.42/5.98	127	2	*Zea mays*	1.359
Carbon and energy metabolism								
R10	gi|460407876	V-type proton ATPase subunit d2-like	41.3/4.9	36.53/4.62	154	6	*Solanum lycopersicum*	-3.684
R11	gi|449454235	Predicted: V-type proton ATPase subunit B 1-like	54.36/4.96	52.22/4.67	393	9	*Cucumis sativus*	6.056
R12	gi|470108902	Predicted: V-type proton ATPase subunit B2-like	54.61/5.07	53.04/4.70	72	8	*Fragaria vesca* subsp. *vesca*	4.146
R16	gi|490262869	ATP synthase subunit D, partial	19.24/5.21	14.44/5.18	102	2	*Hydnora visseri*	1.438
R19	gi|355479515	Adenosine kinase	38.08/5.08	33.59/5.14	104	4	*Medicago truncatula*	3.827
R22	gi|473798701	ATP synthase subunit beta, mitochondrial	57.83/5.25	49.52/5.15	719	10	*Triticum urartu*	1.402
R26	gi|346683384	ATPase subunit 1	55.24/5.58	61.31/6.16	435	11	*Cucumis sativus*	2.206
R29	gi|449434570	Predicted: ATP synthase subunit beta, mitochondrial-like	59.89/0.00	49.56/5.27	121	16	*Cucumis sativus*	5.272
R30	gi|110288667	Enolase, putative, expressed	51.89/5.72	52.95/5.29	492	11	*Oryza sativa* Japonica Group	1.581
R32	gi|398363571	Fructokinase	34.69/5.49	28.6/5.46	123	4	*Actinidia deliciosa*	3.000
R38	gi|527196189	Nucleoside diphosphate kinase	16.48/6.43	52.61/6.17	143	4	*Genlisea aurea*	2.445
Amino acid and protein metabolism								
R7	gi|223532621	Proteasome subunit beta type 6,9, putative	24.91/5.17	18.50/4.78	109	3	*Ricinus communis*	-4.315
R13	gi|315307966	Heat shock protein 90-1	80.45/4.96	67.92/4.85	155	5	*Nicotiana attenuata*	5.239
R14	gi|527187624	Heat shock protein 70	71.62/5.06	67.43/4.92	513	22	*Genlisea aurea*	8.424

Preprints (www.preprints.org) | NOT PEER-REVIEWED | Posted: 7 December 2020 doi:10.20944/preprints202012.0169.v1

R15	gi|223535705	60S ribosomal protein L23, putative	7.17/11.09	11.34/5.12	74	4	*Ricinus communis*	4.451
R23	gi|508784980	TCP-1/cpn60 chaperonin family protein	64.51/5.62	56.16/4.98	159	6	*Theobroma cacao*	2.581
R27	gi|527189531	Protein disulfide-isomerase, partial	38.13/5.26	31.65/5.33	109	4	*Genlisea aurea*	4.561
R33	gi|332656685	S-adenosyethionine synthase 2	43.63/5.67	44.43/5.56	346	7	*Arabidopsis thaliana*	2.857
R34	gi|351722651	Glutamine synthetase cytosolic isozyme 1	38.99/5.46	32.95/5.74	154	5	*Glycine max*	7.338
R40	gi|351722651	Glutamine synthetase cytosolic isozyme 1	38.99/5.46	25.31/6.17	186	6	*Glycine max*	3.97
Stress and defense								
R1	gi|223529085	Peroxidase, putative	19.45/8.6	32.03/4.05	74	1	*Ricinus communis*	-1.056
R17	gi|474311703	L-ascorbate peroxidase 1, cytosolic	27.56/5.85	23.23/5.14	160	4	*Triticum urartu*	1.219
R20	gi|527187175	Monodehydroascorbate reductase	47.2/5.82	39.32/5.12	118	3	*Genlisea aurea*	4.013
R31	gi|427199300	Thioredoxin	13.67/5.76	11.16/5.73	183	4	*Ipomoea batatas*	1.824
R36	gi|223551378	Catalase, putative	113.36/6.84	38.22/5.88	234	11	*Ricinus communis*	3.83
Transcription and signal transduction								
R2	gi|526117762	14-3-3 protein	29.47/4.79	23.65/4.48	132	2	*Vitis vinifera*	1.661
R3	gi|350539221	14-3-3 protein 7	28.91/4.96	24.95/4.33	110	2	*Solanum lycopersicum*	1.531
R4	gi|543176851	14-3-3 protein	29.26/4.66	24.57/4.41	277	7	*Phaseolus vulgaris*	-1.475
R21	gi|527203530	Actin-97	41.95/5.37	41.35/5.15	698	14	*Genlisea aurea*	2.133
R24	gi|473749533	NuA3 HAT complex component NTO1	103.46/7.88	12.9/5.36	63	17	*Triticum urartu*	4.488
R25	gi|375968572	SKP1 protein	17.63/0.00	14.72/5.37	141	5	*Nicotiana tabacum*	-1.983
R28	gi|527203530	Actin-97	41.95/5.37	41.29/5.26	706	16	*Genlisea aurea*	3.076
Other proteins								
R8	gi|508724744	Pathogen-related protein	27.54/5.10	25.65/4.76	64	4	*Theobroma*	-1.063

 doi:10.20944/preprints202012.0169.v1

							cacao	
R39	gi|15239652	Flavodoxin-like quinone reductase 1	21.40/5.96	15.6/6.43	84	2	*Arabidopsis thaliana*	4.289
Unknown proteins								
R5	gi|125562472	Hypothetical protein OsI_30174	16.21/8.51	59.29/4.46	73	6	*Oryza sativa* Indica Group	5.139
R6	gi|226521422	Predicted protein	88.7/5.56	59.7/4.49	68	14	*Micromonas sp. RCC299*	3.272
R9	gi|527206839	Hypothetical protein M569_02468	27.34/9.01	32.97/4.88	76	4	*Genlisea aurea*	-4.319
R18	gi|557113120	Hypothetical protein EUTSA_v10025711mg	34.88/6.07	28.49/5.14	139	4	*Eutrema salsugineum*	-1.621
R35	gi|557531169	Hypothetical protein CICLE_v10012166mg	36.16/9.43	25.17/5.9	140	3	*Citrus clementina*	-3.594

 doi:10.20944/preprints202012.0169.v1

5

6 **Table 3.** Identification of DEPs of *A. mollis* leaves with an expression change greater than 2.0-fold change under tidal flooding stress

Spot [a]	Accession (gb) [b]	Protein Name [c]	Thero. [d] kDa/p*I*	Exper. [e] kDa/p*I*	Score [f]	MP [g]	Species [h]	SF vs. CK [i]
Photosynthesis and photorespiration								
20	gi|543176923	Oxygen-evolving enhancer protein 1	35.20/6.08	19.74/5.42	170	4	*Phaseolus vulgaris*	-2.242
26	gi|474445723	Phosphoglycolate phosphatase	33.22/8.87	24.64/5.41	64	4	*Triticum urartu*	-1.575
33	gi|223539254	Oxygen-evolving enhancer protein 2, chloroplast precursor, putative	28.76/8.63	13.68/5.79	130	4	*Ricinus communis*	-2.109
43	gi|474121685	Chlorophyll a-b binding protein 8, chloroplastic	29.29/8.69	11.86/5.78	109	3	*Triticum urartu*	-2.066
52	gi|223551247	Ferredoxin-NADP reductase, putative	40.74/8.70	14.35/6.50	69	9	*Ricinus communis*	4.265
63	gi|527197786	Cytochrome b6-f complex iron-sulfur subunit 1, chloroplastic, partial	24.25/8.48	11.51/6.78	1.9	4	*Genlisea aurea*	2.970
64	gi|330318806	Photosystem I reaction center subunit iv b	11.37/9.88	12.76/6.95	67	4	*Camellia sinensis*	2.491
Calvin cycle								
3	gi|399139356	Ribulose-1,5-bisphosphate carboxylase/oxygenase large subunit, partial	51.49/6.46	34.61/4.81	654	19	*Anisochilus pallidus*	-4.053
5	gi|335059563	Ribulose-1,5-bisphosphate carboxylase/oxygenase large subunit	34.09/7.83	34.19/4.74	245	3	*Humbertia madagascariensis*	-3.850
14	gi|502137718	Predicted: ribulose bisphosphate carboxylase/oxygenase activase 2, chloroplastic-like	48.07/8.47	40.24/5.02	298	7	*Cicer arietinum*	7.049
15	gi|488888859	Chloroplast rubisco activase 1	48.37/7.66	39.76/5.09	300	4	*Sagittaria graminea*	2.472
21	gi|488888859	Chloroplast rubisco activase 1	48.37/7.66	40.27/5.26	204	5	*Sagittaria graminea*	1.432

 doi:10.20944/preprints202012.0169.v1

22	gi|355488628	Ribulose bisphosphate carboxylase large chain	19.46/4.87	48.33/5.43	72	4	*Medicago truncatula*	-4.455
25	gi|452119476	Ribulose bisphosphate carboxylase large subunit, partial (chloroplast)	47.76/0.00	13.67/5.68	81	8	*Ulva reticulata x Ulva taeniata*	-3.093
27	gi|355513999	Phosphoribulokinase	46.00/6.68	35.60/5.34	118	11	*Medicago truncatula*	-1.498
28	gi|488888860	Chloroplast rubisco activase 2	36.40/6.33	34.77/5.37	178	3	*Sagittaria graminea*	2.933
35	gi|488888859	Chloroplast rubisco activase 1	48.37/7.66	35.45/5.50	283	4	*Sagittaria graminea*	2.256
36	gi|488888860	Chloroplast rubisco activase 2	36.40/6.33	35.35/5.59	212	9	*Sagittaria graminea*	1.143
40	gi|340511990	Ribulose-1,5-bisphosphate carboxylase/oxygenase large subunit, partial(chloroplast)	50.77/6.23	45.85/5.62	337	14	*Scutellaria minor*	-1.418
51	gi|413953335	Transketolase isoform 2	69.06/5.46	68.55/6.07	167	4	*Zea mays*	-1.502
66	gi|399139488	Ribulose-1,5-bisphosphate carboxylase/oxygenase large subunit, partial	51.66/6.19	45.56/6.70	435	14	*Crossandra infundibuliformis*	1.249
Carbon metabolism								
13	gi|404551307	Glyceraldehyde-3-phosphate dehydrogenase, partial	13.46/6.89	49.62/6.82	133	1	*Agave x ajoensis*	-2.462
47	gi|317373797	Chloroplast phosphoglycerate kinase 3	50.28/6.69	46.51/5.79	284	8	*Helianthus annuus*	-1.571
57	gi|449450436	Predicted: glutamate-glyoxylate aminotransferase 2-like	52.90/5.62	56.93/6.31	260	8	*Cucumis sativus*	-3.996
61	gi|530684266	Fructose-bisphosphate aldolase	42.21/6.38	29.80/6.47	345	8	*Oryza sativa* Japonica Group	1.987
65	gi|332645863	Triosephosphate isomerase	27.38/5.39	19.18/4.00	151	4	*Arabidopsis thaliana*	4.485
TCA cycle								
45	gi|461488119	Succinyl-CoA ligase beta-chain	45.40/5.98	36.07/6.05	171	3	*Oryza sativa* Japonica Group	3.395

 doi:10.20944/preprints202012.0169.v1

54	gi|433335660	Malate dehydrogenase	36.04/6.11	26.68/6.35	294	4	*Brassica oleracea*	1.040
62	gi|475577109	Malate dehydrogenase 1, mitochondrial	34.93/5.26	31.95/6.64	96	2	*Aegilops tauschii*	2.970
Energy metabolism								
16	gi|408899417	AtpA, partial (chloroplast)	55.13/5.53	50.63/5.10	315	12	*Mammea americana*	1.179
23	gi|408899391	AtpA, partial (chloroplast)	55.08/5.08	50.50/5.21	514	17	*Erythroxylum areolatum*	-1.452
29	gi|546138044	ATP synthase CF1 alpha subunit (chloroplast)	56.14/5.70	47.94/5.38	163	5	*Cocos nucifera*	-1.203
30	gi|402243685	ATP synthase beta subunit, partial (chloroplast)	49.69/5.11	61.11/5.41	737	9	*Flindersia laevicarpa*	-3.030
31	gi|410176162	ATP synthase CF1 beta subunit (chloroplast)	53.54/5.09	55.39/5.44	939	19	*Origanum vulgare* subsp. *vulgare*	-1.359
37	gi|223535342	Alcohol dehydrogenase, putative	41.61/8.61	32.30/5.63	103	3	*Ricinus communis*	4.043
53	gi|330254337	NAD(P)-binding Rossmann-fold-containing protein	34.97/8.37	21.16/6.41	102	3	*Arabidopsis thaliana*	1.887
Amino acid and protein metabolism								
2	gi|226500014	3-beta hydroxysteroid dehydrogenase/isomerase family protein	32.73/8.34	24.66/4.84	77	1	*Zea mays*	-1.236
10	gi|222863465	Glutamine synthetase family protein	48.20/6.48	30.89/5.24	211	6	*Populus trichocarpa*	1.857
11	gi|223551115	Proteasome subunit alpha type, putative	30.64/4.89	32.86/5.24	192	8	*Ricinus communis*	-2.136
17	gi|226499860	Stromal 70 kDa heat shock-related protein	74.85/5.08	73.19/4.96	259	6	*Zea mays*	-2.046
32	gi|392465167	Heat shock protein 70	71.46/5.14	66.46/5.31	140	4	*Nicotiana tabacum*	2.392
34	gi|527197598	Cysteine synthase	34.65/5.41	27.95/5.71	100	3	*Genlisea aurea*	-3.840
38	gi|226508704	Elongation factor Tu	50.79/6.07	41.71/5.78	184	6	*Zea mays*	-1.312
39	gi|449440632	Predicted: elongation factor Tu,	51.89/5.90	40.25/5.94	94	8	*Cucumis sativus*	-1.458

 doi:10.20944/preprints202012.0169.v1

		chloroplastic-like						
41	gi|508784980	TCP-1/cpn60 chaperonin family protein	64.51/5.62	61.78/5.48	233	3	*Theobroma cacao*	-1.794
44	gi|449506050	Predicted: glutamine synthetase nodule isozyme-like	39.30/5.59	36.26/6.00	75	4	*Cucumis sativus*	3.714
48	gi|543176708	ATP sulfurylase 2-like protein	40.12/0.00	45.36/5.86	253	11	*Phaseolus vulgaris*	-1.428
50	gi|460415276	Predicted: adenosyl homocysteinase-like	53.69/5.78	51.09/6.03	355	9	*Solanum lycopersicum*	-1.435
56	gi|350538867	Arginase 2	36.94/5.60	36.83/6.37	193	8	*Solanum lycopersicum*	1.206
Stress and defense								
1	gi|502111694	Predicted: peroxiredoxin-2E, chloroplastic-like	23.44/7.67	29.05/7.0	125	1	*Cicer arietinum*	-1.189
4	gi|502111694	Predicted: peroxiredoxin-2E, chloroplastic-like	23.44/7.67	36.6/4.86	125	1	*Cicer arietinum*	-5.574
7	gi|511774224	2-Cys peroxiredoxin, partial	25.60/8.51	20.94/4.93	398	11	*Nicotiana benthamiana*	-2.897
12	gi|223533515	Peroxidase 12 precursor, putative	39.40/7.55	35.09/4.94	110	2	*Ricinus communis*	1.136
24	gi|145323784	L-ascorbate peroxidase 1	27.79/5.85	12.32/5.50	376	6	*Arabidopsis thaliana*	-1.521
42	gi|460384911	Predicted: annexin D5-like	35.82/9.05	9.32/6.12	79	14	*Solanum lycopersicum*	2.169
46	gi|222856181	Oxidoreductase family protein	39.33/5.83	39.53/6.28	81	2	*Populus trichocarpa*	3.093
49	gi|508777590	Monodehydroascorbate reductase 6 isoform 4	53.16/8.80	46.57/6.16	337	5	*Theobroma cacao*	-1.598
60	gi|330255786	Glutathione S-transferase phi 8	29.27/0.00	18.84/6.43	83	3	*Arabidopsis thaliana*	2.957
Transcription and signal transduction								
8	gi|514824684	Predicted: fanconi anemia group I protein homolog	153.86/8.00	22.31/5.07	61	13	*Setaria italica*	-1.455

Preprints (www.preprints.org) | NOT PEER-REVIEWED | Posted: 7 December 2020 doi:10.20944/preprints202012.0169.v1

9	gi|12229593	RecName: Full=14-3-3-like protein	29.35/4.79	21.17/5.03	96	2	*Lilium longiflorum*	-1.349
18	gi|412993712	Pre-mRNA-splicing factor 38A	32.52/5.03	11.61/5.28	60	10	*Bathycoccus prasinos*	-4.501
19	gi|474386333	Poly(C)-binding protein 3	37.52/6.76	18.39/5.23	60	10	*Triticum urartu*	3.395
55	gi|449532425	Predicted: chloroplast stem-loop binding protein of 41 kDa, chloroplastic-like, partial	30.27/5.26	29.54/6.23	85	2	*Cucumis sativus*	-1.761
58	gi|384582593	Maturase K, partial (chloroplast)	18.02/9.64	9.50/6.51	66	5	*Poincianella exostemma*	-3.933
67	gi|527203530	Actin-97	41.95/5.37	57.78/6.80	437	12	*Genlisea aurea*	-1.757
Unknown proteins								
6	gi|388503040	Unknown	28.24/5.47	39.35/4.86	75	3	*Medicago truncatula*	-3.176
59	gi|502142675	Predicted: uncharacterized protein LOC101509967 Isoform X1	10.31/4.92	11.97/6.50	62	5	*Cicer arietinum*	3.827

Table 4. Identification of DEPs of *A. mollis* roots with an expression change greater than 2.0-fold change under tidal flooding stress

Spot [a]	Accession (gb)[b]	Protein Name [c]	Thero. [d] kDa/p*I*	Exper. [e] kDa/p*I*	Score [f]	MP [g]	Species [h]	SF vs. CK [i]
TCA cycle								
R22	gi|113622845	Os08g0120000	31.84/8.81	46.91/5.23	62	5	*Oryza sativa* Japonica Group	1.372
R28	gi|470107271	Predicted: succinyl-CoA ligase [ADP-forming] subunit beta, mitochondrial-like	45.39/5.87	34.20/5.76	93	4	*Fragaria vesca* subsp. *vesca*	-3.345
R37	gi|475610756	Succinate dehydrogenase (ubiquinone) flavoprotein subunit, mitochondrial	81.40/6.24	57.35/6.09	98	5	*Aegilops tauschii*	-2.810
Carbon and energy metabolism								
R3	gi|223547542	NADH dehydrogenase, putative	19.14/4.76	12.75/4.50	77	1	*Ricinus communis*	-2.186

 doi:10.20944/preprints202012.0169.v1

R7	gi|223539983	Alpha-galactosidase/alpha-n-acetylgal actosaminidase, putative	40.06/5.19	40.56/4.28	125	6	*Ricinus communis*	-1.844
R10	gi|514802088	Predicted: beta-glucosidase 12-like	51.94/6.73	53.37/4.52	61	12	*Setaria italica*	-3.641
R20	gi|355479515	Adenosine kinase	38.08/5.08	25.56/5.20	103	6	*Medicago truncatula*	1.701
R26	gi|470124373	Predicted: beta-galactosidase 13-like	87.36/8.91	60.62/5.27	63	9	*Fragaria vesca* subsp. *vesca*	-6.185
R30	gi|350538295	Enolase	48.05/5.68	49.90/5.73	301	8	*Solanum lycopersicum*	5.906
R35	gi|550346968	UDP-glucose 4-epimerase family protein	38.44/5.66	31.38/5.99	108	7	*Populus trichocarpa*	-2.385
R36	gi|223525768	Alcohol dehydrogenase, putative	41.88/5.98	43.45/6.38	106	4	*Ricinus communis*	1.372
R39	gi|390098824	Triosephosphate isomerase cytosolic isoform-like	27.31/5.72	16.51/4.00	207	6	*Capsicum annuum*	-2.761
R40	gi|11467928	Cytochrome b	45.52/9.85	24.80/6.69	61	3	*Acutodesmus obliquus*	-2.804
R42	gi|460405093	Predicted: probable aldo-keto reductase 4-like	60.97/5.51	31.89/6.22	76	5	*Solanum lycopersicum*	-1.893
R43	gi|508708397	Thiamin diphosphate-binding fold (THDP-binding) superfamily protein isoform 2	36.04/8.67	35.88/6.31	63	5	*Theobroma cacao*	-2.545
R44	gi|223525768	Alcohol dehydrogenase, putative	41.88/5.98	43.26/6.32	61	5	*Ricinus communis*	2.574
R45	gi|407369264	Alcohol dehydrogenase, partial	20.74/6.08	50.46/6.32	76	1	*Pinus taiwanensis*	1.412
Amino acid and protein metabolism								
R1	gi|460411270	Predicted: 60S acidic ribosomal protein P2B-like isofoR1	11.41/4.55	9.28/4.05	86	1	*Solanum lycopersicum*	-1.880
R11	gi|432140649	Heat shock protein 70	74.29/5.26	72.91/4.58	475	16	*Lactuca sativa*	3.076
R13	gi|430763366	Polyubiquitin 14, partial	15.57/5.74	28.74/4.83	68	2	*Cornus kousa*	-3.358
R14	gi|502126081	Predicted: proteasome subunit alpha type-1-B-like	31.59/4.94	30.00/4.90	100	5	*Cicer arietinum*	-1.714
R15	gi|514761174	Predicted: 26S protease regulatory subunit 6A homolog	47.99/4.94	43.41/4.77	308	14	*Setaria italica*	1.053

 doi:10.20944/preprints202012.0169.v1

R23	gi|334184654	Heat shock protein 60-2	61.78/6.08	60.46/5.14	202	11	*Arabidopsis thaliana*	-3.003
R24	gi|413956514	Glutamine synthetase3	18.23/6.92	35.05/5.36	79	6	*Zea mays*	-2.010
R25	gi|330252829	20S proteasome alpha subunit G1	27.64/5.93	38.92/5.39	62	10	*Arabidopsis thaliana*	1.143
R27	gi|508778822	Tetratricopeptide repeat (TPR)-like superfamily protein, putative	64.56/8.70	50.52/5.61	61	14	*Theobroma cacao*	1.036
R29	gi|355429958	Putative S-adenosyl-L-homocysteinase	61.87/5.69	45.20/5.89	75	8	*Linum usitatissimum*	2.505
R33	gi|527194033	S-formylglutathione hydrolase, partial	24.93/6.22	27.19/6.21	69	2	*Genlisea aurea*	-2.060
R38	gi|502137510	Predicted: 60S ribosomal export protein NMD3-like	59.49/6.07	15.16/6.32	71	14	*Cicer arietinum*	-2.219
Stress and defense								
R2	gi|511774224	2-Cys peroxiredoxin, partial	25.60/8.51	15.21/4.49	77	5	*Nicotiana benthamiana*	-2.780
R17	gi|440573478	Tau class glutathione S-transferase	27.80/7.62	48.05/4.92	63	8	*Pinus tabuliformis*	-3.345
Transcription and signal transduction								
R4	gi|297333574	GF14 omega	29.37/4.70	21.33/4.35	112	4	*Arabidopsis lyrata* subsp. *lyrata*	-2.804
R8	gi|460377572	Predicted: 14-3-3-like protein-like	29.22/4.69	21.08/4.54	84	6	*Solanum lycopersicum*	-1.246
R9	gi|226498758	Inositol-tetrakisphosphate 1-kinase 3	37.72/8.59	41.17/4.47	63	8	*Zea mays*	-2.060
R12	gi|413942896	Profilin-4	14.21/4.63	10.66/4.71	71	2	*Zea mays*	4.448
R21	gi|508715249	Ran-binding protein 1 b isoform 1	25.21/4.70	29.56/4.99	79	2	*Theobroma cacao*	-1.913
R31	gi|508786508	Cell division control 6 isoform 7	47.05/8.95	21.75/6.48	66	14	*Theobroma cacao*	-1.658
R32	gi|223549247	ATP-dependent RNA helicase, putative	78.24/8.86	23.64/6.31	62	16	*Ricinus communis*	1.741
R34	gi|186510546	Ankyrin repeat family protein	87.56/6.52	26.05/6.27	67	11	*Arabidopsis thaliana*	2.089
Photosynthesis								
R18	gi|543177187	RuBisCO large subunit-binding protein subunit alpha, belongs to the	61.28/0.00	54/4.8	147	4	*Phaseolus vulgaris*	-1.076

 doi:10.20944/preprints202012.0169.v1

		chaperonin family						
		Other proteins						
R6	gi|514802368	Predicted: endochitinase A-like	30.18/8.55	39.52/7.00	83	1	*Setaria italica*	3.202
R16	gi|15242097	Putative villin	108.44/5.25	49.09/4.86	60	17	*Arabidopsis thaliana*	-2.169
R19	gi|508787331	Ferritin 4	30.44/6.56	17.58/4.99	116	8	*Theobroma cacao*	5.694
Unknown proteins								
R5	gi|300256770	Hypothetical protein VOLCADRAFT_119802	87.21/5.31	32.42/4.25	61	9	*Volvox carteri f. nagariensis*	-3.003
R41	gi|162688983	Predicted protein	38.61/8.27	30.98/6.42	63	8	*Physcomitrella patens* subsp. *patens*	-1.472

[a] The spot number corresponding to the number listed in the table 1-4. R represents the root tissue. Underlined numbers represent *A. mollis* tissues.

[b] Database accession numbers (gb) according to NCBInr.

[c] The name of proteins was identified by LC-MALDI-TOF/TOF.

[d] Theoretical mass (kDa) and p*I* of identified proteins. Theoretical values were retrieved from the NCBInr database.

[e] Experimental mass (kDa) and p*I* of identified proteins. Experimental values were calculated by using PDquest software and standard molecular mass markers.

[f] The Mascot searched score against the database NCBInr.

[g] Number of matched peptide fragments.

[h] The species that has the high homology of the identified protein.

[i] Log_2- (fold change) values between the different treatments. SF vs CK means soil flooding treatment vs control group.

Preprints (www.preprints.org) | NOT PEER-REVIEWED | Posted: 7 December 2020 doi:10.20944/preprints202012.0169.v1

2.5. Identification of hub proteins in Acanthus species

Because of the lack of genome information on *A. ilicifolius* and *A. mollis*, the DEPs of the two species were annotated based on the existing NR database. Based on our previous studies (Li et al. 2020) and homologous protein distribution analysis (Supplementary Fig. S3), *Arabidopsis thaliana* was used to assemble the PPI network of *A. ilicifolius* and *A. mollis*. The top-ten hub proteins were identified with a degree score of CytoHubba and displayed in Figure 6. The hub proteins of *A. ilicifolius* tissues were mostly associated with carbon and energy metabolism (Fig. 6A, B), whereas those of the *A. mollis* tissues were mostly associated with photosynthesis and photorespiration and the TCA cycle (Fig. 6C, D).

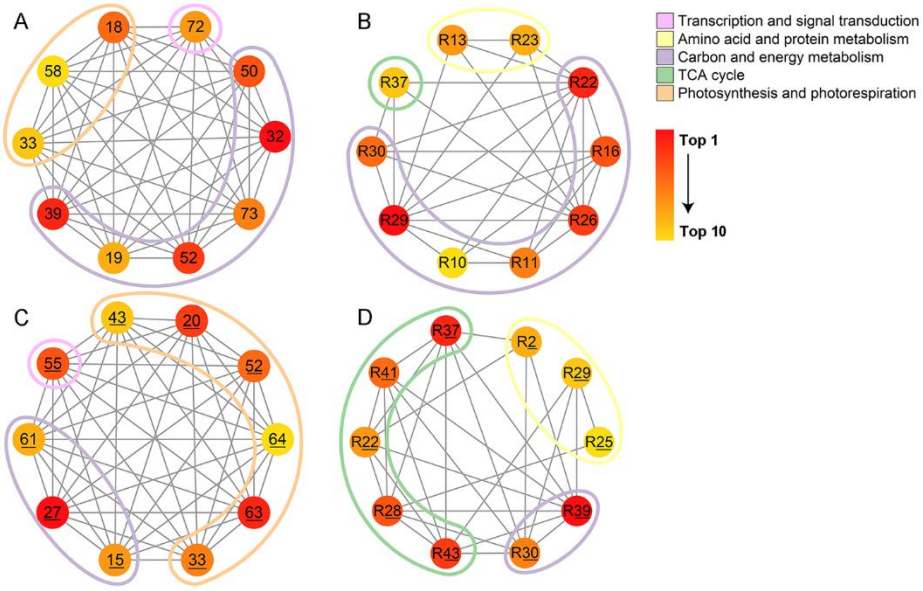

Fig. 6. Top 10 hub proteins in network of (A) *A. ilicifolius* leaves, (B) *A. ilicifolius* roots, (C) *A. mollis* leaves, (D) *A. mollis* roots ranked by Matthews correlation coefficient (MCC) method. R represents the root tissue. Underlined numbers represent *A. mollis* tissues.

2.6. Tidal flooding stress influences the energy status level of A. ilicifolius and A. mollis

The further comparison demonstrated that *A. mollis* had a higher AMP, ADP, and ATP content than *A. ilicifolius* in the control group (Fig. 7A-C). *A. ilicifolius* promptly responded to flooding stress by significantly increasing ADP and ATP contents in the leaves (Fig. 7B-C). However, AMP and ATP contents were significantly decreased in *A. mollis* roots (Fig. 7B-C) under tidal flooding stress. The energy charge represents the energy status of biological cells [24]. Whereas the energy charge of *A. ilicifolius* roots was significantly increased under tidal flooding stress, it was significantly decreased in *A. mollis* tissues (Fig. 7D).

Preprints (www.preprints.org) | NOT PEER-REVIEWED | Posted: 7 December 2020 doi:10.20944/preprints202012.0169.v1

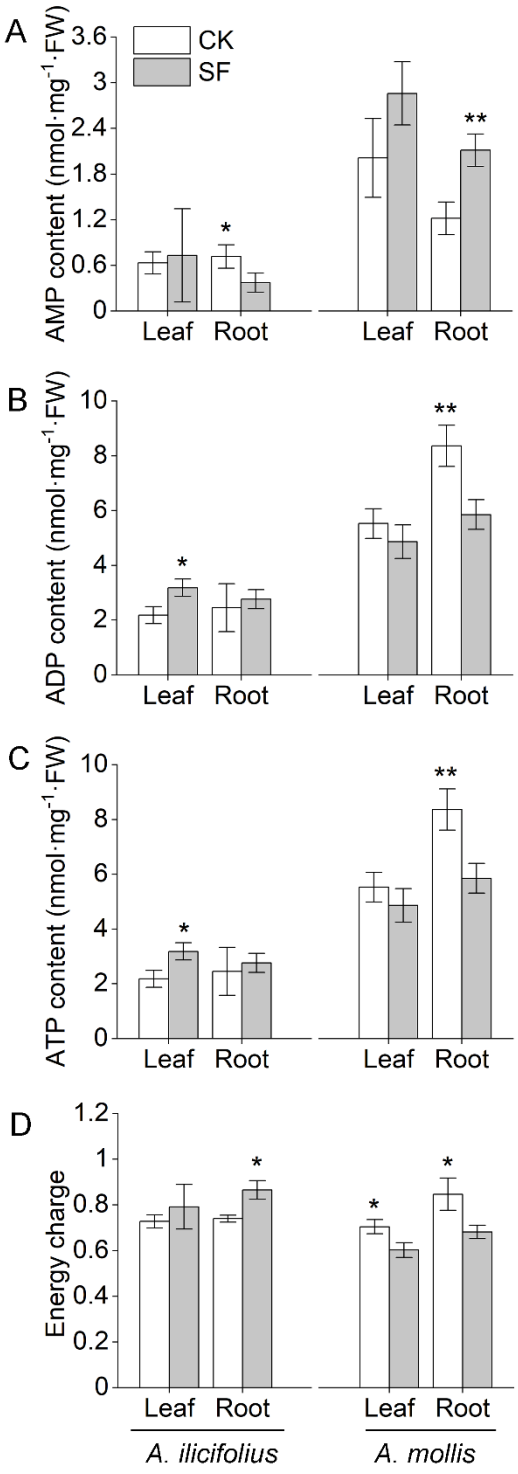

Fig. 7. Effects of tidal flooding stress on (A) AMP content, (B) ADP content, (C) ATP content, and (D) energy charge of *A. ilicifolius* and *A. mollis*. * and ** indicate significant difference at the 0.05 level and the 0.01 level, respectively. CK and SF represent the control group and soil tidal flooding stress, respectively.

2.7. Tidal flooding stress influences the total soluble sugar and starch contents of Acanthus species

There was no significant change in the content of total soluble sugar and starch of *A. ilicifolius* tissues under tidal flooding stress (Fig. 8A-B). Nevertheless, there was significant tidal flooding tolerance in the ratio of soluble sugar to starch in *A. ilicifolius* tissues (Fig. 8C). The total soluble sugar

Preprints (www.preprints.org) | NOT PEER-REVIEWED | Posted: 7 December 2020 doi:10.20944/preprints202012.0169.v1

content, starch content, and the ratio of soluble sugar to starch were lower in *A. mollis* tissues than in the control group, except for the ratio of soluble sugar to starch in the leaves (Fig. 8A-C).

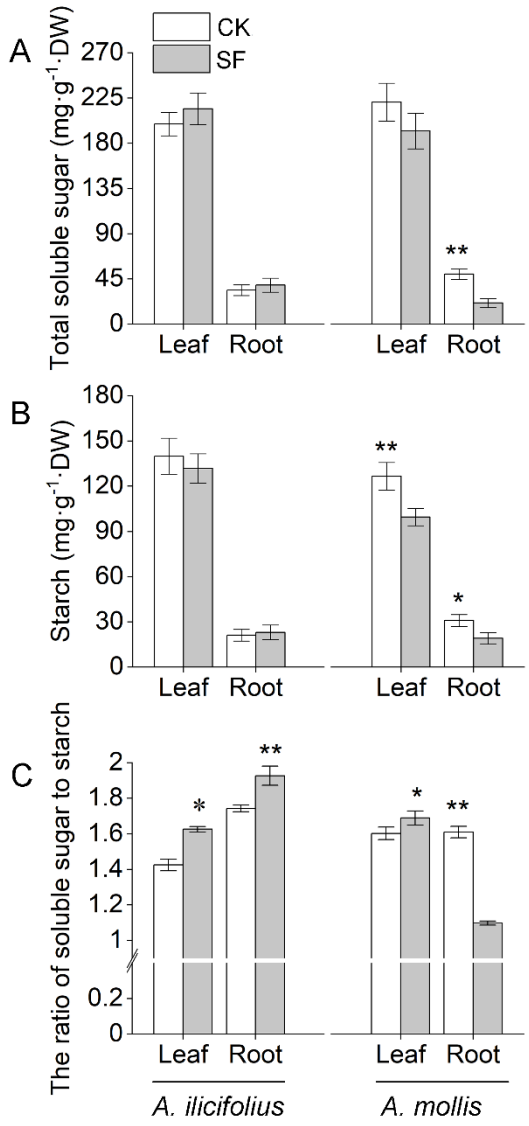

Fig. 8. The concentration of soluble sugar, starch and the ratio of soluble sugar to starch for *A. ilicifolius* and *A. mollis* under tenth day tidal flooding stress. * and ** indicate significant difference at the 0.05 level and the 0.01 level, respectively. CK and SF represent control and soil tidal flooding stress, respectively.

2.8. qRT-PCR validation of the abundance of proteins

The genes were selected for real-time PCR analysis to confirm the reliability of protein abundance in this study. The details of these genes and their specific primers are shown in Supplemental Table S1. The results showed that most of the gene expressions in *A. ilicifolius* and *A. mollis* were strongly correlated with protein abundance (Fig. 9), confirming the reliability of the protein data.

Preprints (www.preprints.org) | NOT PEER-REVIEWED | Posted: 7 December 2020 doi:10.20944/preprints202012.0169.v1

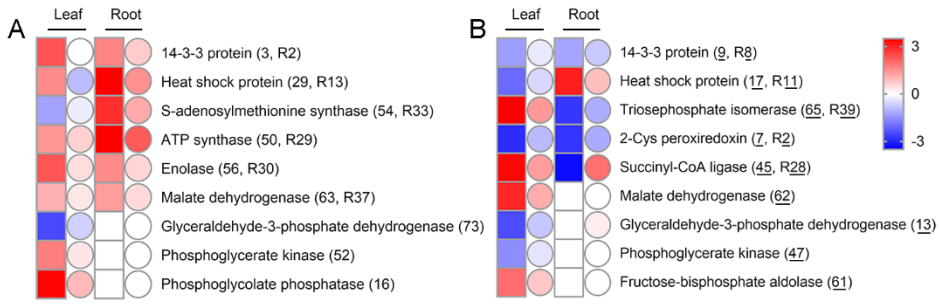

Fig. 9. Proteins levels confirmation by mRNA. Ten genes (Table S1) of (A) *A. ilicifolius* and (B) *A. mollis* were selected for analysis the correlation between the protein abundance and mRNA levels. Protein abundance is depicted by square and mRNA levels are depicted by circle. Red indicates up-regulation and blue indicates down-regulation.

3. Discussion

3.1. Differences in tissue tolerance between Acanthus species

Unlike previous findings in the mangrove, *A. marina*, seedlings [25], the upper and lower epidermises of *A. ilicifolius* showed no change with prolonged waterlogging duration in the present study (Fig. 1B2, B3). The leaf anatomical features of *A. mollis* were also relatively less susceptible to tidal flooding stress within a short span. The leaf anatomy plays an important role in determining photosynthetic capacity. Herbaceous plants with high photosynthetic capacity usually have thinner epidermis, leading to high values of mesophyll conductance [26]. The mangrove leaf exhibited a range of xeromorphic features, including thick epidermis and wax coatings [25]. Therefore, like other mangrove plants, *A. ilicifolius* leaves are likely to regulate the Calvin cycle to resist the tidal flooding stress (Table 1). A comparative analysis showed that palisade and spongy tissue that were loosely arranged with large spaces and epidermis were thinner in *A. mollis* leaf, making CO_2 entry easier.

A. ilicifolius, mainly distributed in the foreshore seaward region, was found to develop a high percentage of schizogenous aerenchyma to facilitate efficient internal oxygen transfer [27]. According to previous study, the mangrove species appeared to higher waterlogging tolerance when the aerenchyma formation was induced [28]. The aortic root anatomy of *A. ilicifolius* was not affected by the tidal flooding stress. The special anatomical structure of roots was not the main reason for *A. ilicifolius* to tolerance tidal flooding stress at the early stage. Water and minerals transport from the root system to the aerial portions via the xylem tissue. The phloem translocates photosynthetic products from mature leaves to roots and redistributes water and various compounds throughout the plant body [29]. In *A. mollis*, the aortic root anatomy exhibited broken xylem, phloem, and periderm tissues, indicating a negative influence on the allocation and partitioning of photosynthetic products (Fig. 1 C4, D4).

3.2 Effect of tidal flooding on the photosynthesis of Acanthus species

The proportion of photosynthesis-related proteins within the total DEPs of *A. ilicifolius* leaves was close to that of *A. mollis* leaves (Fig. 5). Most hub proteins of *A. mollis* leaves were associated with photosynthesis (Fig. 6C). The abundance of oxygen-evolving enhancer protein (OEE, spot 18) showed an increasing trend in *A. ilicifolius* leaves under tidal flooding stress. Oxygen-evolving complex (OEC) proteins are degraded and release OEE as a degradation product to promote the plant to adapt to the adverse conditions [30]. OEE is a subunit of the OEC of photosystem II in the chloroplast [31] considered to be directly involved in photosynthesis. It is suggested that decreased OEE abundance (spot 20, 33) might negatively affect *A. mollis* leaves.

Chlorophyll a/b-binding protein (light-harvesting complex, LHC) captures light in the light reaction [32]. Root hypoxia suppressed photosynthetic activity by decreasing the expression of LHC in pea leaves [33]. Most of chlorophyll a/b-binding proteins increased in *A. ilicifolius* leaves (spot 12,

Preprints (www.preprints.org) | NOT PEER-REVIEWED | Posted: 7 December 2020 doi:10.20944/preprints202012.0169.v1

13, 58) but decreased in *A. mollis* leaves (spot 43) under tidal flooding stress. However, electron transport chain proteins, such as ferredoxin-nicotinamide adenine dinucleotide phosphate (NADP) reductase (spot 52), cytochrome b6-f complex iron-sulfur subunit 1 (spot 63), and photosystem I reaction center subunit IV b (spot 64), increased in *A. mollis* leaves, promoting photosynthetic electron transport under tidal flooding stress [31]. One fraction of the captured light energy is used to reduce $NADP^+$ to reduced nicotinamide adenine dinucleotide phosphate (NADPH) and the other fraction is used for light-dependent ATP synthesis. The proteomic data showed that chloroplast ATP synthesis was decreased in *A. mollis* leaves (spot 23, 29, 30, 31). ATP-dependent zinc metalloprotease FTSH2 (FtsH2, spot 41, 42), which is involved in the turnover of the ΦPSII reaction center D1 protein [34], was increased in maize to protect chloroplast photosynthesis under heat stress [35]. Herein, increased FtsH2 abundance had a positive effect on tidal flooding tolerance of *A. ilicifolius* leaves.

3.3 Effect of tidal flooding on carbon and energy metabolism of Acanthus species

It is well known that the photosynthetic system and its maintenance can severely affect plant survival under an abiotic stress environment [36]. Therefore, to meet the increased demands for survival, plants change their energy metabolism pathways.

3.3.1. Calvin cycle

The reactions catalyzing the reduction of CO_2 to carbohydrates are coupled to the consumption of ATP and NADPH by enzymes found in the stroma, the soluble phase of chloroplasts. Therefore, we compared Calvin cycle-related proteins between the two species to determine their CO_2 fixation ability under tidal flooding stress. The activation state of Rubisco, a key enzyme in the Calvin cycle, is regulated by Rubisco activase [37]. RuBisCO activase increased in both *A. ilicifolius* (spot 5 and 19) and *A. mollis* (spot 14, 15, 21, 28, 35, and 36). The abundance of RuBisCO large subunits increased in *A. ilicifolius* (spots 7, 9, and 15) but decreased in *A. mollis* (spots 3, 5, 22, 25, and 40); the protein abundance showed a different change between the two species. A similar result was observed in *Trifolium* species, the waterlogging sensitive species exhibited a higher reduction of Rubisco large subunits expression [36].

3.3.2. Sugar metabolism

CO_2 fixation is performed through the Calvin cycle to drive sugar production and energy storage in plants [35]. A higher soluble sugar concentration (Figure 8A) in flooded *A. ilicifolius* plant is not solely due to photosynthesis but also the conversion of carbohydrates from starch to sugar (Figure 8C). We found that *A. ilicifolius* roots in the abundance of fructokinase (spot R32) exhibited a 3.0-fold increase compared with controls in response to tidal flooding treatment. Fructokinase regulates starch synthesis coordinately with sucrose synthase and plays a key role in starch accumulation in tomato fruit [38]. Decreased alpha-galactosidase (spot R7) and beta-galactosidase (spot R26) abundance, which are crucial in catalyzing galactose to useful products utilized in cell wall metabolism [39-40], had adverse effects on *A. mollis* roots under tidal flooding stress. Meanwhile, beta-glucosidase (spot R10) and UDP-glucose 4-epimerase family protein (spot R35) were also decreased, indicating that the induction of polysaccharide catabolism and the interconversion of hexoses (glucose/galactose) were inhibited in *A. mollis* roots under tidal flooding stress [41-42].

3.3.3. Glycolysis, TCA cycle, and ethanol fermentation

Total soluble sugar and starch contents, as the carbon source, were stored and used for cell respiration [43]. Carbohydrates metabolism, especially glycolysis and the TCA cycle, mainly provides energy for plant growth and development [44]. Pyruvate produced via the glycolytic pathway into the TCA cycle and the consequent electrons is transferred along an electron transport chain and then return to the mitochondrial matrix via ATP synthase [45].

Preprints (www.preprints.org) | NOT PEER-REVIEWED | Posted: 7 December 2020 doi:10.20944/preprints202012.0169.v1

Most of the glycolysis and TCA cycle-related proteins were increased in *A. ilicifolius* tissues under tidal flooding stress, including triosephosphate isomerase (spot 34 and 46), phosphoglycerate kinase (spot 38, 49, and 52), enolase (spot 56, 68, and R30), malate dehydrogenase (spot 63, 64, and R37), and dihydrolipoamide dehydrogenase (spot 74). In *A. mollis*, the abundance of glycolysis and TCA cycle-related proteins mostly showed an increase in leaves and a decrease in the roots under tidal flooding stress. Similar to the proteomic data of a previous study [21], increased glycolysis and TCA cycle-related protein abundances contributed to the defense system of *A. marina* leaves under short-term inundation. The chemical energy conserved during the TCA cycle in form of nicotinamide adenine dinucleotide (NADH) and flavin adenine dinucleotide (FADH2) (redox equivalents with high-energy electrons) is converted to ATP, which plays a key role in the cell [45]. This process occurs in the inner mitochondrial membrane and is accomplished by ATP synthesis. Interestingly, we found that mitochondrial ATP synthase was decreased in *A. ilicifolius* leaves (spot 24, 32) but increased in *A. ilicifolius* roots (spot R16, R22, R26, R29), indicating that the requirement of ATP decreased accordingly. This implied that high levels of ATP synthase abundance might not be needed in *A. ilicifolius* leaves. Our study revealed the presence of vacuolar H+-ATPase (V-ATPase) subunit in *A. ilicifolius* tissues (spots 6, 43, 44, R10, R11, and R12). Increased V-ATPase abundance was helpful to maintain the cytosolic pH homeostasis and provide free energy to establish a proton motive force across membranes in *A. ilicifolius* tissues [46]. Physiological data showed the ATP level or energy charge of the *A. ilicifolius* tissues was increased to tolerance the tidal flooding stress (Fig. 5C, D).

Aldehyde dehydrogenase is involved in fermentation along with alcohol dehydrogenase (ADH) [47]. Due to the low efficiency of energy conservation under fermentation, an increased rate of glycolysis is required to sustain ATP production necessary for cell survival [48]. We found that the abundance of ADH (spot R36, R44, R45) increased with a concomitant reduction in glycolysis and TCA cycle-related proteins (spot R28, R37) in *A. mollis* roots under tidal flooding stress. Glycolysis converts glucose to pyruvate for the production of energy [45]. Thiamine diphosphate (spot R43), a co-factor of upregulated pyruvate, showed a decrease in *A. mollis* roots [49], indicating a reduction of pyruvate level. Physiological data showed the ATP level and energy charge of *A. mollis* roots became too low to sustain the basal metabolic requirement of roots (Fig. 5C, D).

3.4 Effect of tidal flooding on nutrient assimilation and protein metabolism of Acanthus species

Sugar metabolism provides sufficient energy to amino acid metabolism and intermediates from glycolysis can be utilized as precursors for the synthesis of amino acids [50]. In *A. ilicifolius* leaves and roots, many up-regulated proteins were associated with amino acid and protein metabolism (Fig. 5).

Nitrogen utilization is an important physiological activity in plant growth and development [48]. Increased abundances of glutamine synthetase (spot 53), glutamate-ammonia ligase family protein (spot 66, R34, R40), and glycine dehydrogenase (spot 75, 76) were considered to contribute to the conversion of ammonium generated from nitrate assimilation or photorespiration into amino acids in the cell of *A. ilicifolius* tissues. In *A. mollis* tissues, nitrogen metabolism-related enzymes, such as glutamine synthetase (spot 10, 44) and arginase (spot 56), showed an increase in leaves. Inhibited arginase activity led to the blockage of the nitrogen reutilization pathway in rice [51], indicating the promotion of nitrogen reutilization by increasing arginase abundance in *A. mollis* leaves.

S-adenosyl methionine synthetase (SAMS) catalyzes the biosynthesis of S-adenosyl-L-methionine (SAM) via the methionine cycle to participate in ethylene biosynthesis [50]. Overexpressed SAMS increased the ethylene level of *A. thaliana* [52], suggesting that the production of ethylene would be reduced in leaves and promoted in roots by tidal flooding stress. Meanwhile, MTA/SAH nucleosidase (spot 37), which showed an increase in *A. ilicifolius* leaves, promoted methionine recycling under tidal flooding stress [53]. Methionine is metabolized to homocysteine via SAM and SAH intermediates [54]. In the present study, tidal flooding stress influenced the abundance of SAH in *A. mollis*, which was decreased in the leaves (spot 50) but

Preprints (www.preprints.org) | NOT PEER-REVIEWED | Posted: 7 December 2020 doi:10.20944/preprints202012.0169.v1

increased in the roots (spot R29). In addition, decreased sulfate adenylyltransferase (spot 48) and cysteine synthase (spot 34) abundances indicated adverse effects on producing cysteine from sulfate in *A. mollis* leaves [12, 55]. Overall, the sulfate assimilation pathway that feeds the biosynthesis of cysteine is suppressed in *A. mollis* leaves.

Plant tissue exposure to abiotic stress induces protein damage in cells. Therefore, plant broke down damaged proteins for cell survival [56]. Increased proteasome subunit alpha type (spot 17) and proteasome subunit beta type (spot 59) abundances were observed in *A. ilicifolius* under tidal flooding stress. Both DEPs are subunits of the 26S proteasome that was involved in the direct degradation of misfolded or oxidized proteins or via the ubiquitin-proteasomal pathway [57]. Furthermore, heat shock proteins (spots 10, 11, 26, 28, 29, and R13) mostly increased in *A. ilicifolius* under tidal flooding stress. These DEPs participates in plant fitness mainly by folding mature protein or degrading misfolded proteins [58]. Metabolism-related proteins in *A. ilicifolius* facilitate normal protein folding and guard the proteome against misfolding and aggregation under tidal flooding stress. In *A. mollis*, the abundance of proteasome subunit alpha type (spot 11, R14) and polyubiquitin (spot R13) were decreased but 26S protease regulatory subunit 6A homolog (spot R15) and 20S proteasome alpha subunit (spot R25) increased during the flooding stage.

In addition, protein synthesis essentially requires ribosomes, which play a distinct role in all living cells [59]. The biogenesis of 40S ribosomal subunits was enhanced by increasing RNA-binding protein NOB1 (spot 47) abundance in *A. ilicifolius* leaves. The tidal flooding stress decreased 60S ribosomal-related proteins (spot R1, R38) abundance, suggesting inhibition of protein synthesis in *A. mollis* roots. In *A. ilicifolius* roots, tidal flooding stress increased protein disulfide isomerase (spot 27) abundance, which is a molecular chaperone containing thioredoxin domains that help in the formation of disulfide bonds during protein folding [60].

3.5 Effect of tidal flooding on antioxidative defense system of Acanthus species

The antioxidative defense system has a stronger reactive oxygen scavenging capacity to mitigate oxidative damage under flooding stress [61]. Our data suggested that most of the antioxidant enzyme-related proteins, including l-ascorbate peroxidase (spot 36, R17), thioredoxin (spot R15, R31), monodehydroascorbate reductase (spot R20), and catalase (spot R36), were increased in *A. ilicifolius* under tidal flooding stress. The ascorbate-glutathione cycle together with 2-Cys peroxiredoxin is relevant systems in detoxifying reactive oxygen in stressed plants [62]. It has been reported that most of the enzymes (spot 2, R7, 24, and 49) involved in this process decrease in *A. mollis*.

In addition, annexin genes have been reported to have peroxidase activity [63]; it has been hypothesized that elevated abundance of annexin D5-like (spot 42) together with glutathione S-transferase (spot 60) modulate endogenous ROS levels in *A. mollis* leaves under tidal flooding stress. Moreover, glutathione S-transferase in protein regulation via S-glutathionylation, as a post-translational modification, have been reported in plants [64].

3.6 Effect of tidal flooding on transcription and signal transduction of Acanthus species

According to Ka/Ks ratios, 14-3-3 protein was a positive selection gene of *Acanthus* species, which plays an essential role in species survival in complex environments [15]. 14-3-3 protein is not only involved in signal transduction but also takes part in the regulation of carbon and nitrogen metabolism [65]. In soybean, the expression of 14-3-3 protein improved flooding resistance [66]. In the current study, the abundance of 14-3-3 protein increased in *A. ilicifolius* (spot 3, 14, R2, and R3) but decreased in *A. mollis* (spot 9, R4, and R8) under tidal flooding stress. As a secondary messenger to multiple signals response, inositol-tetrakisphosphate 1-kinase (spot R9) was decreased, indicating tidal flooding stress damage of the signal pathway of *A. mollis* roots.

Some redox-sensitive proteins involved in cellular structure, such as actin, profilin-4, tubulin α, and annexin D5-like, were found in *Acanthus* species. A previous study demonstrated that actin could be an important functional protein to response environmental factors [67]. Although actin filaments respond to UV-B radiation by influencing the process of mitosis, their dynamics are

Preprints (www.preprints.org) | NOT PEER-REVIEWED | Posted: 7 December 2020 doi:10.20944/preprints202012.0169.v1

disrupted by salinity stress [65]. The actin abundance increased in *A. ilicifolius* leaves (spot 40, R21, R28) but decrease in *A. mollis* leaves (spot 67) to respond to tidal flooding stresses. Moreover, protein tubulin α (spot 22), which is also involved in mitosis, showed an increase in *A. ilicifolius* leaves. Therefore, although increased profilin-4 (spot R12) abundance stabilized the actin structure of *A. mollis* roots, we observed an increase in cell division-related proteins in *A. ilicifolius* leaves (spot 41, 42) and a decrease in *A. mollis* roots (spot R31).

4. Materials and Methods

4.1 Plant material and experimental setup

Experiment materials were obtained from vegetative propagation. The stems of *A. ilicifolius* (9-12 mm in diameter and 10-20 cm in length) were collected from the Zini mangrove forest (117°91 E, 24°45′ N), south of the Jiulong River Estuary, Fujian Province, China. The roots of *A. mollis* were collected from a mother plant that was planted in the greenhouse for one year. The explants of *A. ilicifolius* and *A. mollis* were placed in pots (19 cm in diameter and 20 cm in depth) with soil plus vermiculite in a ratio of 3:1. The growth of cuttings is shown in Supplementary Fig. S1. 1/8-strength Hoagland nutrient solution with rooting hormone powder was used to promote the growth of stems and adventitious roots. In the first two months, the cuttings were grown under controlled conditions: temperature (28 ± 2℃), weak light, and relative humidity (60 ± 5%). The pots were then transferred to a new condition with 1000 μmol·m^{-2}·s^{-1} light intensity, 12 h light period day^{-1}, and 28 ± 2℃ temperature.

After growth for five months, uniform and healthy plants were selected for further analysis. The plants were randomly divided into two groups. The soil water content of the control group was kept at 65 ± 5% and regulated by the oven drying method. The pots were placed inside 50 L plastic containers maintaining a 1-2 cm water layer above the soil surface (Supplementary Fig. S2) and treated with flooding stress for 6 h per day. All the pots perforated at the bottom to ensure proper drainage. The dry weight of the leaves and roots samples were taken every two days. The extraction of protein and RNA, paraffin sectioning, and the measurement of energy (adenosine monophosphate (AMP), adenosine diphosphate (ADP), ATP), and hydrogen peroxide (H_2O_2) content were performed on the tenth day.

4.2 Determination of the dry weight

Five plants were randomly selected, washed with distilled water, and divided into two parts (leaves and roots). The oven-dried (at 70°C for 72 h) leaves and roots samples were measured for dry weight in grams (g) using an electric weight balance. The tidal flooding tolerance of each species was determined as the relative plant dry weight (dry weight under tidal flooding treatment divided by dry weight under control conditions, expressed as a percentage). Each measurement was repeated three times with five replications per treatment.

4.3 Anatomical features of leaves and roots

The leaf center and mature root were collected from *A. ilicifolius* and *A. mollis* for paraffin sectioning. The fresh tissues were fixed in formalin-acetic acid-alcohol (FAA) solution containing 70% ethanol, 5% acetic acid, and 4% paraformaldehyde for 72 h. Then, tissues were fixed and dehydrated in an ethanol series (50-100%). Tissues were cleared by xylene and embedded by paraffin (58℃). Paraffin-embedded tissue blocks were sectioned with 10 mm thickness, and then cross-sections were stained with 1% aqueous safranin and 0.5% fast green. Tissues sections were photographed under a light microscope (Leica DM4 P, Germany) to determine anatomical parameters.

4.4 Protein extraction and quantification

Preprints (www.preprints.org) | NOT PEER-REVIEWED | Posted: 7 December 2020 doi:10.20944/preprints202012.0169.v1

Protein extraction was according to the method described by He and Wang [68] with some modifications. After 10 days of tidal flooding treatment, 2-4 g of treated tissue from *A. ilicifolius* and *A. mollis* were ground in liquid nitrogen and extracted using the tricarboxylic acid (TCA)-acetone/phenol-methanol combined extraction method. The tissue powder was transferred to a centrifuge tube and precipitated by adding cold acetone solution containing 0.2% dithiothreitol (DTT), and then centrifuged at 6000 rpm for 20 min at 4°C. The supernatant was discarded and the pellet was suspended in the 2× extraction buffer (20 mM Tris-HCl (pH 8.0), 250 mM sucrose, 10 mM ethylene glycol tetraacetic acid, 1 mM phenylmethylsulfonyl fluoride, 1% Triton X-100, 2% β-mercaptoethanol) at 4°C for 15 min. Then the homogenate was vortexed at 4°C for 15 min by adding an equal volume of saturated phenol (pH 7.5). The homogenate was centrifuged at 12000 rpm for 30 min to obtain the upper phenol phase and then mixed with three volumes of ice-cold methanol (containing 0.1 M ammonium acetate). After overnight precipitation at -20°C, the mixture was centrifuged at 12000 rpm and discarded the supernatant. Then the pellet was washed once with ammonium acetate/methanol (0.1M) and thrice with acetone (containing 0.2% DTT). Protein quantification was performed using the Bradford [69] method with bicinchoninic acid as the standard. Each treatment was performed for three biological replications for quantitative analysis.

Gel strips (Immobiline Dry Strip, pH 4-7,17cm; Bio-Rad, Hercules, CA) and 12.5% polyacrylamide gels were used to separate the prepared samples in the first and second dimension, respectively. The first dimension was performed with an Ettan IPG phor system (GE Healthcare Amersham Bioscience, Little Chalfont, UK). The second dimension was accomplished using Bio-Rad PROTEAN XL/PowerPac (Bio-rad, USA). The sodium dodecyl sulfate-polyacrylamide gel electrophoresis (SDS-PAGE) gels were stained with Coomassie Brilliant Blue R-250 and scanned with Uniscan M3600 (China) at 600 dpi. Gels were analyzed using PDQuest software (Version 8.0, Bio-Rad). The DEPs were obtained by pairwise comparison with a fold change ≥2.0 and a Student's t-test ($p<0.05$). In-gel tryptic digestion and protein identification were performed according to the method of Liu et al. [70].

4.5 Determinations of AMP, ADP, ATP, and sugar content

The method of ATP, ADP, and AMP extraction was according to Chen et al. [71] with some modifications. The powder was obtained from 2 g tissue and then homogenized with 10 ml perchloric acid (0.6 mol·L^{-1}) at 4℃ for 30 min. Then the extraction mixture was centrifuged at 6000 rpm for 20 min. The resulting supernatant (6 ml) was quickly neutralized to pH 6.5-6.8 with 1 mol·L^{-1} potassium hydroxide solution and passed through a 0.22-μm syringe filter. The supernatant was diluted to 10 ml before measuring. Shimadzu® LC-20A Prominence high-performance liquid chromatography (HPLC) equipped with Syncronis C18 column (4.6 mm × 250 mm, Thermo Fisher Scientific) was used to measure ATP, ADP, and AMP contents. The mobile phase was 0.1% phosphoric acid and the flow rate was 0.8 mL·min^{-1}. The ultraviolet detection wavelength was 254 nm. The energy charge (EC) was calculated using the following formula: EC = ([ATP] + 1/2 [ADP])/([ATP] + [ADP] + [AMP]). Data were expressed as means of the five replicates.

The starch and total soluble sugar contents were measured with the starch content kit and plant soluble sugar content test kit, respectively (Nanjing Jian Cheng Institute, Nanjing, China).

4.6 RNA extraction and gene expression analysis

Total RNA was extracted from 0.05 g of fresh tissues according to the manufacturer's instructions using a MiniBEST plant RNA extraction kit (TaKaRa, Tokyo, Japan). The quality of RNA was examined by 1% (w/v) agarose gel electrophoresis. RNA was reverse-transcribed into cDNA using TaqMan™ reverse transcription reagents (Invitrogen, Life Technologies) and stored the cDNA at -80°C for further analysis. Primers were designed based on gene sequences listed in National Center for Biotechnology Information (NCBI) and transcriptome data from Yang et al. [15]. The primer sequences are provided in Supplemental Table S1.

Quantitative reverse transcription-polymerase chain reaction (qRT-PCR) was performed using Bio-Rad CFX96 (USA) in 25 μL volumes, containing 12.5 μL 2× FastSYBR Mixture (CWbiotech,

China), 1 μL primers, 1 μL of the cDNA, and 10.5 μL RNase-free water. The amplification condition was initial denaturation (94°C for 10 min) followed by 40 cycles (30 s at 94°C, 30 s at 61°C, and 45 s at 72°C). The result was calculated using the $2^{-\Delta\Delta CT}$ method [72]. The relative gene expression was assayed along with β-actin as a reference gene and run in five biological repetitions.

4.7 Data analysis

The experimental data were evaluated with IBM SPSS Statistics for Mac (Version 23.0). The gels were analyzed using PDQuest software (Version 8.0, Bio-Rad). Principal Component Analysis (PCA) was performed using the OmicShare tools, a free online platform for data analysis (http://www.omicshare.com/tools). The classification of identified proteins was performed using the UniProt Knowledgebase (http://www.uniprot.org) and the NCBI (https://www.ncbi.nlm.nih.gov). The protein-protein interaction (PPI) network analysis was acquired using the Search Tool for the Retrieval of Interacting Genes/Proteins (STRING) version 11.0 (https://string-db.org). Cytoscape software of the PPI network can visualize significant protein-protein associations [73]. The Cytoscape plugin (cytoHubba) was utilized to evaluate hub proteins from the PPI network by Matthews correlation coefficient (MCC) method [73]. We used the degree score to identify hub proteins.

5. Conclusions

Physiological and proteomic analyses have greatly enriched the current knowledge of flooding resistance in *Acanthus* species. *A. ilicifolius* performed better under tidal flooding stress, which was reflected in the integrity of the morphological structure, a high level of energy charge, and an increase in the ratio of soluble sugar to starch. A higher percentage of up-regulated proteins associated with carbon and energy metabolism were found in *A. ilicifolius* tissues under tidal flooding stress. However, the change in the root structure was not responsible for adaption to flooding conditions at the early stage and the maintenance of physiological homeostasis had higher demands for essential supply of energy. *A. mollis* leaves remained structurally intact even after tidal flooding stress, which might be due to partially enhanced ROS scavenging capacity and carbon and energy metabolism. The disruption of energy provision and flux balance in *A. mollis* roots demonstrates that maintenance of an energy balance under abiotic stress is critical for cell survival. As shown in Figure 10, we propose a working model to illustrate the detailed mechanism of *A. ilicifolius* and *A. mollis* under tidal flooding stress.

Supplementary Materials: Supplementary materials can be found at www.mdpi.com/xxx/s1.

Funding: This research was funded by the National Key Research and Development Program of China (2017YFC0506102), and the Natural Science Foundation of China (NSFC 31570586 and 31870581).

Conflicts of Interest: The authors declare no conflict of interest.

References

1. Arbona V., Hossain Z., López-Climent M.F., Pérez-Clemente R.M., Gómez-Cadenas A. Antioxidant enzymatic activity is linked to waterlogging stress tolerance in citrus. *Physiol. Plantarum.* **2008**, 132, 452-466.
2. Vandoorne B., Descamps C., Mathieu A.S., Van den Ende W., Vergauwen R., Javaux M., Lutts S. Long term intermittent flooding stress affects plant growth and inulin synthesis of Cichorium intybus (var. sativum). *Plant Soil* **2014**, 376, 291-305.
3. García-Sánchez F., Syvertsen J.P., Gimeno V., Botía P., Perez-Perez J.G. Responses to flooding and drought stress by two citrus rootstock seedlings with different water-use efficiency. *Physiol. Plant* **2007,** 130, 532-542
4. Gibbs J., Greenway H. Mechanisms of anoxia tolerance in plants. I. Growth, survival and anaerobic catabolism. *Funct. plant Biol.* **2003**, 30, 1-47.

5. Kotula L., Clode P.L., Striker G.G., Pedersen O., Läuchli A., Shabala S., Colmer T.D. Oxygen deficiency and salinity affect cell-specific ion concentrations in adventitious roots of barley (H ordeum vulgare). *New Phytol.* **2015**, 208, 1114-1125
6. Azahar I., Ghosh S., Adhikari A., Adhikari S., Roy D., Shaw A.K., Singh K., Hossain Z. Comparative analysis of maize root sRNA transcriptome unveils the regulatory roles of miRNAs in submergence stress response mechanism. *Environ. Exp. Bot.* **2020**, 171, 103924.
7. Pedersen O., Rich S.M., Colmer T.D. Surviving floods: leaf gas films improve O2 and CO2 exchange, root aeration, and growth of completely submerged rice. *Plant J* **2009**, 58, 147-156.
8. Cheng H., Wang Y.S., Fei J., Jiang Z.Y., Ye Z.H. Differences in root aeration, iron plaque formation and waterlogging tolerance in six mangroves along a continues tidal gradient. *Ecotoxicology* **2015**, 24, 1659-1667.
9. Garcia N., Da-Silva C.J., Cocco K.L.T., Pomagualli D., de Oliveira F.K., da Silva J.V.L., de Oliveira A.C.B., do Amarante L. Waterlogging tolerance of five soybean genotypes through different physiological and biochemical mechanisms. *Environ. Exp. Bot.* **2020**, 172, 103975.
10. Van Dongen J.T., Licausi F. Oxygen Sensing and Signaling. *Annu. Rev. Plant Biol.* **2015**, 66, 345-367.
11. Luo F.L., Nagel K.A., Zeng B., Schurr U., Matsubara S. Photosynthetic acclimation is important for post-submergence recovery of photosynthesis and growth in two riparian species. *Ann. Bot.* **2009**, 104, 1435-1444.
12. Ploschuk R.A., Grimoldi A.A., Ploschuk E.L., Striker G.G. Growth during recovery evidences the waterlogging tolerance of forage grasses. *Crop Pasture Sci.* **2017,** 68, 574-582.
13. Li A.M., Wei C.X., Jiang J.J., Zhang Y.T., Snowdon R.J., Wang Y.P. Phenotypic variation in progenies from somatic hybrids between Brassica napus and Sinapis alba. *Euphytica* **2009**, 170, 289-296.
14. Hansen L.N., Earle E.D. Somatic hybrids between Brassica oleracea L. and Sinapis alba L. with resistance to *Alternaria brassicae* (Berk.) Sacc. *Theor. Appl. Genet* **1997,** 94, 1078-1085.
15. Yang Y.C., Yang S.H., Li J.F., Deng Y.F., Zhang Z., Xu S.H., Guo W.X., Zhong C.R., Zhou R.C., Shi S.H. Transcriptome analysis of the holly mangrove *Acanthus ilicifolius* and its terrestrial relative, *Acanthus leucostachyus*, provides insights into adaptation to intertidal zones. *BMC Genomics* **2015,** 16, 605.
16. Shackira A.M., Puthur J.T. Cd2+ influences metabolism and elemental distribution in roots of *Acanthus ilicifolius* L. *Int. J. Phytoremediat* **2019**, 21, 866-877.
17. Zhang L.E., Liao B.W., Guan W. Effects of simulated tide inundation on seed germination and seedling growth of mangrove species *Acanthus ilicifolius*. *Chin. J. Ecol.* **2011**, 30, 2165-2172
18. Řezanka T., Řezanka P., Sigler K. Glycosides of arylnaphthalene lignans from *Acanthus mollis* having axial chirality. *Phytochemistry* **2009**, 70, 1049-1054
19. Matos P., Figueirinha A., Ferreira I., Cruz M.T., Batista M.T. *Acanthus mollis* L. leaves as source of anti-inflammatory and antioxidant phytoconstituents. *Nat. prod. Res.* **2019,** 33, 1824-1827.
20. Bader A., Martini F., Schinella G.R., Rios J.L., Prieto J.M. Modulation of cox-1, 5-, 12- and 15-lox by popular herbal remedies used in southern Italy against psoriasis and other skin diseases. *Phytother. Res.* **2015,** 29, 108-113.
21. Li H., Li Z., Shen Z.J., Luo M.R., Liu Y.L., Wei M.Y., Wang W.H., Qin Y.Y., Gao C.H., Li K.K., Ding Q.S., Zhang S., Zhang X.M., Gao G.F., Zhu X.Y., Zheng H.L. Physiological and proteomic responses of mangrove plant *Avicennia marina* seedlings to simulated periodical inundation. *Plant Soil* **2020**, 450, 231-254.
22. Campilho A., Nieminen K., Ragni L. The development of the periderm: the final frontier between a plant and its environment. *Curr. Opin. Plant Biol.* **2020**, 53, 10-14.
23. Yi T., Zhu L., Peng W.L., He X.C., Chen H.L., Li J., Yu T., Liang Z.T., Zhao Z.Z., Chen H.B. Comparison of ten major constituents in seven types of processed tea using HPLC-DAD-MS followed by principal component and hierarchical cluster analysis. *LWT-Food Sci. Technol.* **2015**, 62, 194-201.
24. Chen Y.R., Chen C.L., Zhang L.W., Green-Church K.B., Zweier J.L. Superoxide generation from mitochondrial NADH dehydrogenase induces self-inactivation with specific protein radical formation. *J. Biol. Chem.* **2005**, 280, 37339-37348.
25. Xiao Y., Jie Z.L., Wang M., Lin G.H., Wang W.Q. Leaf and stem anatomical responses to periodical waterlogging in simulated tidal floods in mangrove *Avicennia marina* seedlings. *Aquat. Bot.* **2009,** 91, 231-237.
26. Hassiotou F., Ludwig M., Renton M., Veneklaas E.J., Evans J.R. Influence of leaf dry mass per area, CO2, and irradiance on mesophyll conductance in sclerophylls. J. Exp. Bot. **2009,** 60, 2303-2314.

27. Pi N., Tam N.F.Y., Wu Y., Wong M.H. Root anatomy and spatial pattern of radial oxygen loss of eight true mangrove species. *Aquat. Bot.* **2009,** 90, 222-230.
28. Cheng H., Wu M.L., Li C.D., Sun F.L., Sun CC, Wang Y.S. Dynamics of radial oxygen loss in mangroves subjected to waterlogging. *Ecotoxicology* **2020,** 29, 684-690.
29. McGarry R.C., Kragler F. Phloem-mobile signals affecting flowers: applications for crop breeding. Trends *Plant Sci.* **2013,** 18, 198-206.
30. Downton W.J.S., Loveys B.R., Grant W.J.R. Non-uniform stomatal closure induced by water stress causes putative non-stomatal inhibition of photosynthesis. *New Phytol.* **2006,** 110, 503-509.
31. James H.E., Bartling D., Musgrove J.E., Kirwin P.M., Herrmann R.G., Robinson C. Transport of proteins into chloroplasts. Import and maturation of precursors to the 33-, 23-, and 16-kDa proteins of the photosynthetic oxygen-evolving complex. *J. Biol. Chem.* **1989,** 264, 19573-19576.
32. Alboresi A., Le Quiniou C., Yadav S.K., Scholz M., Meneghesso A., Gerotto C., Simionato D., Hippler M., Boekema E.J., Croce R., Morosinotto T. Conservation of core complex subunits shaped the structure and function of photosystem I in the secondary endosymbiont alga Nannochloropsis gaditana. *New Phytol.* **2017**, 213, 714-726.
33. Ladygin V.G. The effect of root hypoxia and iron deficiency on the photosynthesis, biochemical composition, and structure of pea chloroplasts. *Russ. J. Plant Physiol.* **2004,** 51, 28-40
34. Kato Y., Miura E., Ido K., Ifuku K., Sakamoto W. The variegated mutants lacking chloroplastic FtsHs are defective in D1 degradation and accumulate reactive oxygen species. *Plant Physiol.* **2009**, 151, 1790-1801
35. Zhao F.Y., Zhang D.Y., Zhao Y.L., Wang W., Yang H., Tai F.J., Li C.H., Hu X.L. The difference of physiological and proteomic changes in maize leaves adaptation to drought, heat, and combined both Stresses. *Front Plant Sci.* **2016**, 7, 1471.
36. Stoychev V., Simovastoilova L., Vaseva I., Kostadinova A., Nenkova R., Feller U., Demirevska K. Protein changes and proteolytic degradation in red and white clover plants subjected to waterlogging. *Acta. Physiol. Plant* **2013**, 35, 1925-1932.
37. Takahashi H., Takahara K., Hashida S., Hirabayashi T., Fujimori T., Kawai-Yamada M., Yamaya T., Yanagisawa S., Uchimiya H. Pleiotropic modulation of carbon and nitrogen metabolism in Arabidopsis plants overexpressing the NAD kinase2 gene. *Plant physiol.* **2009**, 151, 100-113.
38. Odanaka S., Bennett A.B., Kanayama Y. Distinct physiological roles of fructokinase isozymes revealed by gene-specific suppression of Frk1 and Frk2 expression in tomato. *Plant Physiol.* **2002**, 129, 1119-1126
39. Eda M., Ishimaru M., Tada T., Sakamoto T., Kotake T., Tsumuraya Y., Mort A.J., Gross K.T. Enzymatic activity and substrate specificity of the recombinant tomato β-galactosidase 1. *J. Plant Physiol.* **2014**, 171, 1454-1460.
40. Dai N., Petreikov M., Portnoy V., Katzir N., Pharr D.M., Schaffer A.A. Cloning and expression analysis of a UDP-Galactose/Glucose pyrophosphorylase from melon fruit provides evidence for the major metabolic pathway of galactose metabolism in raffinose oligosaccharide metabolizing plants. *Plant Physiol.* **2006**, 142, 294-304.
41. Ishiyama N., Creuzenet C., Lam J.S., Berghuis A.M. Crystal Structure of WbpP, a genuine UDP-N-acetylglucosamine 4-epimerase from Pseudomonas aeruginosa Substrate specificity in UDP-hexose 4-epimerases. *J. Biol. Chem.* **2004,** 279, 22635-22642
42. Qiao F., Kong L., Peng H., Huang W., Wu D., Liu S., Clarke J.L., Qiu D., Peng D.L. Transcriptional profiling of wheat (*Triticum aestivum* L.) during a compatible interaction with the cereal cyst nematode Heterodera avenae. *Sci. Rep-UK* **2019,** 9, 2184.
43. Xiao W.Y., Sheen J., Jang J.C. The role of hexokinase in plant sugar signal transduction and growth and development. *Plant Mol. Biol.* **2000**, 44, 451-461.
44. Rocha M., Licausi F., Araujo W.L., Nunes-Nesi A., Sodek L., Fernie A.R., van Dongen J.T. Glycolysis and the tricarboxylic acid cycle are linked by alanine aminotransferase during hypoxia induced by waterlogging of Lotus japonicus. *Plant Physiol.* **2010,** 152, 1501-1513.
45. Andre C., Froehlich J.E., Moll MR, Benning C. A. Heteromeric plastidic pyruvate kinase complex involved in seed oil biosynthesis in Arabidopsis. *Plant Cell* **2007**, 19, 2006-2022.
46. Arino J., Ramos J., Sychrova H. Alkali metal cation transport and homeostasis in yeasts. *Microbiol. Mol. Biol. Rev.* **2010**, 74, 95-120.
47. Saika H., Matsumura H., Takano T., Tsutsumi N., Nakazono M. A point mutation of Adh1 gene is involved in the repression of coleoptile elongation under submergence in rice. *Breeding Sci.* **2006**, 56: 69-74.

48. Zabalza A., van Dongen J.T., Froehlich A., Oliver S.N., Faix B., Gupta K.J. Schma¨lzlin E., Igal M., Orcaray L., Royuela M., Geigenberger P. Regulation of respiration and fermentation to control the plant internal oxygen concentration. *Plant physiol.* **2009**, 149, 1087-1098.
49. Muller Y.A., Lindqvist Y., Furey W., Schulz G.E., Schneider G. A thiamin diphosphate binding fold revealed by comparison of the crystal structures of transketolase, pyruvate oxidase and pyruvate decarboxylase. *Structure* **1993**, 1, 95-103.
50. Wang L., Fu J.L., Li M., Fragner L., Weckwerth W., Yang P.F. Metabolomic and proteomic profiles reveal the dynamics of primary metabolism during seed development of Lotus (Nelumbo nucifera). *Front. Plant Sci.* **2016,** 7, 750.
51. Li L.L., Zhao J.Y., Zhao Y.N., Lu X., Zhou Z.H., Zhao C.X., Xu G.W. Comprehensive investigation of tobacco leaves during natural early senescence via multi-platform metabolomics analyses. Sci. *Rep-UK,* **2016**, 6, 37976.
52. Kim S.H., Kim S.H., Palaniyandi S.A., Yang S.H., Suh J.W. Expression of potato S-adenosyl-L-methionine synthase (SbSAMS) gene altered developmental characteristics and stress responses in transgenic Arabidopsis plants. *Plant Physiol. Biochem.* **2015,** 87, 84-91.
53. Tedder M.E., Nie Z., Margosiak S., Chu S., Feher V.A., Almassy R., Appelt K., Yager K.M. Structure-based design, synthesis, and antimicrobial activity of purine derived SAH/MTA nucleosidase inhibitors. *Bioorg. Med Chem. Lett.* **2004**, 14, 3165-3168.
54. Roje S. S-Adenosyl-L-methionine: beyond the universal methyl group donor. *Phytochemistry* **2006**, 67, 1686-1698.
55. Vauclare P., Suter M., Sticher L., Ballmoos P.V., Krähenbühl U., Camp R.O.D., Brunold C. Flux control of sulphate assimilation in Arabidopsis thaliana: adenosine 5'-phosphosulphate reductase is more susceptible than ATP sulphurylase to negative control by thiols. *Plant J.* **2010**, 31, 729-740.
56. Schramm F., Ganguli A., Kiehlmann E., Englich G., Walch D., von Koskull-Döring P. The heat stress transcription factor HsfA2 serves as a regulatory amplifier of a subset of genes in the heat stress response in Arabidopsis. *Plant Mol. Biol.* **2006**, 60, 759-772.
57. Kim M.H., Jeon J., Lee S., Lee J.H., Gao L., Lee B.H., Park J.M., Kim Y.J., Kwak J.M. Proteasome subunit RPT2a promotes PTGS through repressing RNA quality control in Arabidopsis. *Nat. plants* **2019**, 5, 1273-1282.
58. Torres M.A., Dangl J.L. Functions of the respiratory burst oxidase in biotic interactions, abiotic stress and development. *Curr. Opin. Plant Biol.* **2005**, 8, 397-403.
59. Boni I.V., Isaeva D.M., Musychenko M.L., Tzareva N.V. Ribosome-messenger recognition: mRNA target sites for ribosomal protein S1. *Nucleic. Acids Res.* **1991**, 19,155-162.
60. Gruber C.W., Čemažar M., Heras B., Martin J.L., Craik D.J. Protein disulfide isomerase: the structure of oxidative folding. *Trends Biochem. Sci.* **2006**, 31, 455-464.
61. Ji X.L., Gai Y.P., Zheng C.C., Mu Z.M. Comparative proteomic analysis provides new insights into mulberry dwarf responses in mulberry (Morus alba L.). *Proteomics* **2010**, 9, 5328-5339.
62. Sun Y.K., Jang H.H., Lee J.R., Sung N.R., Lee H.B., Lee D.H., Park D.J., Kang C.H., Chung W.S., Lim C.O. Yun D.J.; Kim W.Y.; Lee K.O.; Lee S.Y. Oligomerization and chaperone activity of a plant 2-Cys peroxiredoxin in response to oxidative stress. *Plant Sci.* **2009**, 177, 227-232.
63. Góngora-Castillo E., Ibarra-Laclette E., Trejo-Saavedra D.L., Rivera-Bustamante R.F. Transcriptome analysis of symptomatic and recovered leaves of geminivirus-infected pepper (Capsicum annuum). *Virol J.* **2012**, 9, 295.
64. Dixon D.P., Skipsey M., Edwards R. Roles for glutathione transferases in plant secondary metabolism. *Phytochemistry* **2010**, 71, 338–350.
65. Roberts M.R., Salinas J., Collinge D.B. 14-3-3 proteins and the response to abiotic and biotic stress. *Plant Mol. Biol.* **2002**, 50, 1031-1039.
66. Wang X., Khodadadi E., Fakheri B., Komatsu S. Organ-specific proteomics of soybean seedlings under flooding and drought stresses. *J. Proteomics* **2017**, 162, 62-72
67. Chen H.Z., Han R. Characterization of actin filament dynamics during mitosis in wheat protoplasts under UV-B radiation. *Sci Rep-UK* **2016**, 6, 20115.
68. He C.F., Wang Y.M. Protein extraction from leaves of Aloe vera L., a succulent and recalcitrant plant for proteomic analysis. *Plant Mol. Biol. Rep.* **2008**, 26, 292-300.
69. Bradford M.M., Bradford M. A rapid and sensitive method for the quantification of microgram quantities of proteins utilizing the principle-dye binding. *Anal Biochem*. **1976**, 72, 248-254.

 doi:10.20944/preprints202012.0169.v1

70. Liu Y.L., Shen Z.J., Simon M., Li H., Ma D.N., Zhu X.Y., Zheng H.L. Comparative proteomic analysis reveals the regulatory effects of H2S on salt tolerance of mangrove plant *Kandelia obovata*. *Int. J. Mol. Sci.* **2020**, 21, 118.
71. Chen Y., Lin H.T., Jiang Y.M., Zhang S., Lin Y.F., Wang Z.H. Phomopsis longanae Chi-induced pericarp browning and disease development of harvested longan fruit in association with energy status. *Postharvest Biol. Technol.* **2014**, 93, 24-28.
72. Bustin S.A., Benes V., Garson J.A., Hellemans J., Huggett J., Kubista M., Mueller R., Nolan T., Pfaffl M.W., Shipley G.L., Vandesompele J., Wittwer C.Y. The MIQE guidelines: minimum information for publication of quantitative real-time PCR experiments. *Clin. Chem.* **2009**, 55, 611-622.
73. Chin C.H., Chen S.H., Wu H.H., Ho C.W., Ko M.T., Lin C.Y. CytoHubba: identifying hub objects and sub-networks from complex interactome. *BMC Syst. Biol.* **2014**, 8, S11